Wiley
Journal of Food Biochemistry
Volume 2026, Article ID 2627240, 21 pages
https://doi.org/10.1155/jfbc/2627240

WILEY

Research Article

Edible and Medicinal *Fritillaria thunbergii* Miq. Aqueous Extract Improves Metabolic Health via Modulation of Gut Microbiota in Mice Fed on a High-Sugar and High-Fat Diet

Linen Zou,[1] Yu Fu,[1] Lanna Wu,[2] Jiale Cheng,[1] Yanan Yang,[1] Mingxi Li,[1] Yuru Xu,[1] Yan Jiang,[1] Qingchun Wang,[3] and Chongming Wu[1,4]

[1]*School of Chinese Materia Medica, Tianjin University of Traditional Chinese Medicine, Tianjin 301617, China*
[2]*Department of Mongolian Medicine, Hohhot Hospital of Traditional Chinese Medicine and Mongolian Medicine, Hohhot 010050, China*
[3]*Centre of Experimentation, The Inner Mongolia Academy of Traditional Chinese and Mongolian Medicine, Hohhot 010010, China*
[4]*State Key Laboratory of Chinese Medicine Modernization, Research Institute of Traditional Chinese Medicine, Tianjin University of Traditional Chinese Medicine, Tianjin 301617, China*

Correspondence should be addressed to Qingchun Wang; w_youth@outlook.com and Chongming Wu; chomingwu@163.com

Received 21 December 2024; Revised 30 October 2025; Accepted 12 December 2025

Academic Editor: Hongxun Tao

Copyright © 2026 Linen Zou et al. Journal of Food Biochemistry published by John Wiley & Sons Ltd. This is an open access article under the terms of the Creative Commons Attribution License, which permits use, distribution and reproduction in any medium, provided the original work is properly cited.

Fritillaria thunbergii Miq. (FTM), a traditional medicinal and edible herb, has shown promise in alleviating metabolic disturbances, yet its mechanistic basis remains unclear. In this study, we investigated the therapeutic effects of FTM aqueous extract in a male KM mouse model of obesity induced by a high-sugar, high-fat diet (HSFD). A 7-week intervention with FTM significantly ameliorated obesity-related phenotypes, including weight gain, insulin resistance, hyperlipidemia, and histopathological damage in the liver and pancreas. Comprehensive RT-qPCR profiling of 38 hepatic genes revealed coordinated modulation of lipid metabolism (e.g., SREBP1 and FAS), insulin signaling (e.g., IRS1 and GLUT2), inflammation (e.g., NF-κB and IL-10), and mitochondrial function (e.g., PGC-1α), indicating transcriptional reprogramming as a core mechanism. UPLC-QTOF-MS identified eight cevanine-type alkaloids—including peimine, peiminine, and their glycosides—as major constituents, potentially contributing to the observed bioactivity via anti-inflammatory and metabolic regulatory pathways. Moreover, 16S rRNA sequencing demonstrated that FTM reshaped gut microbiota composition by enriching SCFA-producing taxa such as *Lachnospiraceae* and *Faecalibaculum* while suppressing *Akkermansia* overgrowth. Functional predictions further indicated normalization of microbial metabolic pathways disrupted by HSFD. These findings demonstrate that FTM exerts systemic benefits through the integrated modulation of hepatic gene networks, bioactive phytochemicals, and gut microbial communities, supporting its development as a multitarget functional food for the management of glycolipid metabolic disorders.

Keywords: *Fritillaria thunbergii* Miq.; glycolipid metabolism; gut microbiota; high-sugar high-fat diet

Highlight

- *Fritillaria thunbergii* Miq. extract ameliorates HSFD-induced glycolipid metabolic disorders in a dose-dependent manner.
- The extract reprograms hepatic gene expression involved in lipogenesis, insulin signaling, inflammation, and mitochondrial function.
- UPLC-QTOF-MS identifies eight cevanine-type alkaloids, including peimine and peiminine, as key bioactive compounds.
- FTM restores gut microbiota composition and function by enriching beneficial taxa and microbial metabolic pathways.
- The coordinated modulation of the liver–gut–microbiota axis highlights FTM's potential as a multitargeted functional food.

1. Introduction

Fritillaria thunbergii Miq. (FTM), commonly known as *Zhebei*, is a plant recognized for its dual role as both food and medicine, as designated by the National Health Commission of China. Widely cultivated in Zhejiang Province, FTM has been traditionally incorporated into local culinary practices [1], often prepared in soups or broths due to its mild flavor and rich nutritional content [2, 3]. In parallel, it has been extensively used in traditional Chinese medicine for its notable bioactive properties, including anti-inflammatory, antitussive, and antioxidative effects [4]. As the main components of FTM, peimine and peiminine present outstanding anti-inflammatory and antioxidant effects [5, 6]. This unique overlap of nutritional and therapeutic attributes positions FTM as a promising candidate for functional food development. Because chronic inflammation and oxidative stress are associated with multiple metabolic dysfunctions, it is plausible to speculate that FTM may play a role in ameliorating abnormal glycolipid metabolism. Nevertheless, this assumption requires further validation, and the related mechanism also remains to be investigated.

A growing number of metabolic diseases, such as obesity, type 2 diabetes, and nonalcoholic fatty liver disease, are attracting global attention [7]. The abnormal glycolipid metabolism is among the commonest pathophysiological mechanisms of metabolic diseases [8]. This has raised concerns about the adverse effects of excessive fat and sugar consumption [9]. Generally, the high-sugar and high-fat diet (HSFD) can disrupt metabolic equilibrium, further resulting in chronic inflammation, insulin resistance, and dyslipidemia [10]. Despite various agents having recently been developed to control metabolic diseases [11, 12], the strategies for the management of abnormal metabolism at the beginning but not yet diagnosed as disease are still scarce. This necessitates finding new substances for effective glycolipid metabolism management, especially medicinal and food homologous substances.

As is widely known, gut microbiota participate in modulating numerous host metabolic processes, including energy balance, lipid metabolism, and immune responses [13, 14]. Meanwhile, compelling evidences have confirmed that TCMs can mitigate several diseases like ulcerative colitis [15, 16], hyperlipidemia [17], and depression [18] via regulating gut microbiota. There is growing evidence that plant-based compounds can alter bacterial populations, potentially restoring metabolic balance in conditions exacerbated by HSFDs [19]. For instance, short-chain fatty acid (SCFA)-producing bacteria *Lachnospiraceae* family can maintain gut barrier integrity, exert anti-inflammatory effects, and improve lipid metabolism [20]. Therefore, modulating the abundance of beneficial taxa by FTM could be one way to exert FTM's therapeutic effects on metabolic health.

To clarify FTM against abnormal glycolipid metabolism and explore its potential mechanism, we fed mice with HFSD for 7 weeks and detected their serum lipid profiles, hepatic lipid accumulation, and insulin sensitivity. Simultaneously, we conducted detailed analysis of their gut microbiota composition. This study aims to verify the potent beneficial metabolic effect of FTM and proposed one of the potential mechanisms based on gut microbiota. Furthermore, by establishing FTM as both a nutritional and bioactive resource, this study contributes to a new medicinal and food homologous agent for HSFD-introduced abnormal glycolipid metabolism.

2. Materials and Methods

2.1. Preparation of FTM Extract. FTM was sourced from Beijing Tong Ren Tang Health Pharmaceutical Co., Ltd. (Beijing, China). A total of 100 g of the raw material was ground and sieved, followed by the addition of 1 L of distilled water at a solid-to-liquid ratio of 1:10 (g/mL). The mixture was subjected to reflux extraction for 2 h. The resulting extract was filtered through a double-layered gauze, and the filtrate was concentrated at 50°C to a final volume of 100 mL. Subsequently, the concentrated solution was centrifuged at 4000 rpm for 10 min to remove precipitates, and the supernatant was collected and stored at −20°C for future use.

According to the Chinese Pharmacopoeia (2020 edition), the recommended clinical dose of FTM for humans is 10 g, which is equivalent to a dosage of 1.3 g/kg in mice. In this study, low and high doses were set at 0.65 and 1.3 g/kg, respectively.

2.2. UPLC-QTOF-MS Analysis. The chemical profiling of the FTM aqueous extract was performed using an ultra-performance liquid chromatography coupled with a quadrupole time-of-flight mass spectrometry (UPLC-QTOF-MS) system (Xevo G2 QTOF, Waters Corp., USA), equipped with an ACQUITY UPLC HSS T3 column (100 × 2.1 mm, 1.8 μm, Waters, USA). The mobile phase consisted of 0.1% formic acid in water (A) and acetonitrile (B), with the following gradient elution program: 0–1 min, 95%–85% A; 1–7 min, 85%–70% A; 7–9 min, 70%–60% A; 9–11 min, 60%–40% A; 11–17 min, 40%–30% A; 17–19 min, 30%–5% A; 19–22 min, 5%–5% A; 22–22.5 min, 5%–95% A; 22.5–26 min, 95%–95% A. The flow rate was set at 0.3 mL/min, the column

temperature was maintained at 40°C, and the injection volume was 2 μL.

Mass spectrometry was performed using an electrospray ionization (ESI) source operating in both positive and negative ion modes. The ESI (+) conditions were as follows: capillary voltage 3.0 kV, cone voltage 40 V, source temperature 100°C, desolvation temperature 250°C, cone gas flow 50 L/h, and desolvation gas flow 600 L/h. The ESI (−) conditions were as follows: capillary voltage 2.5 kV, cone voltage 40 V, source temperature 100°C, desolvation temperature 250°C, cone gas flow 50 L/h, and desolvation gas flow 627 L/h. The mass range was set to m/z 100–1500 with a scan time of 0.2 s, and collision energy was ramped from 20 to 30 eV for MS/MS acquisition.

Data acquisition and processing were conducted using MassLynx v4.2 software (Waters Corp.). Compounds were annotated by comparing retention time, accurate mass, and fragmentation patterns of the sample with those of reference standards (peimine and peiminine) and by consulting chemical databases such as PubChem (https://pubchem.ncbi.nlm.nih.gov). For compound assignment, a mass error threshold of < 10 ppm was applied, except for peiminine.

2.3. Animal Experiment. Thirty-two male KM mice (5 weeks old, 32–34 g) were obtained from SPF (Beijing) Biotechnology Co., Ltd. and housed under SPF conditions at the Tianjin University of Traditional Chinese Medicine (24 ± 1°C, 50%–70% humidity, 12 h light/dark cycle). Randomization was used to allocate experimental units to control and treatment groups. The randomization sequence was generated using a computer-based random number generator. Potential confounders such as the order of treatments and animal location were controlled. Treatments were administered in the same order each day, and animals were housed in the same position throughout the study. All animal experiments were performed following the ARRIVE guidelines. The experimental protocol was approved by the Animal Experiment Ethics Committee of the Tianjin University of Traditional Chinese Medicine (No. TCM-LAEC2023211z1516, Tianjin, China). Humane endpoints were established to ensure the well-being of the animals. Mice were monitored daily for signs of distress such as excessive weight loss (> 20%), lethargy, difficulty moving, and labored breathing. Any animals exhibiting these signs would have been euthanized. No animals reached humane endpoints during the study, and the monitoring frequency was daily.

Mice were randomized into four groups: normal diet (ND, $n = 6$), HSFD ($n = 6$), and low-dose (FTML, $n = 6$) and high-dose (FTMH, $n = 6$) FTM groups. Over 7 weeks, the ND group received distilled water and standard chow, while HSFD, FTML, and FTMH groups received a 10% fructose solution and high-fat feed (67% standard chow, 10% lard, 20% sucrose, 2.5% cholesterol, 0.5% sodium cholate, SPF (Beijing) Biotechnology Co., Ltd.). The FTML and FTMH groups received FTM extract by gavage for 49 days, while ND and HSFD groups received saline. The outcome measures assessed in this study include body weight and blood glucose levels, which were used to determine the success of the model. These measures were the primary criteria for confirming the induction of metabolic disorders.

At the end of the study, all mice were euthanized by inhalation anesthesia using isoflurane, followed by blood collection via eyeball extirpation. Liver, pancreas, and colon tissues were collected after cardiac perfusion with PBS. One portion of the tissue was stored in 4% paraformaldehyde for fixation, and another portion was stored at −80°C for detection. Feces were also stored at −80°C for full-length 16S rRNA sequencing.

2.4. Examination of Blood Glucose and Lipid Profile. On the 49th day of the experiment, blood was collected from the tail vein, and the fasting blood glucose (FBG) level of each mouse was assessed with a single touch glucometer (ACCU-CHEK Instant S). The serum lipid levels, including total cholesterol (TC, Cat# A111-1-1), triglycerides (TG, Cat# A110-1-1), low-density lipoprotein cholesterol (LDL-c, Cat# A113-1-1), and high-density lipoprotein cholesterol (HDL-c, Cat# A112-1-1), were measured using lipid assay kit as per the manufacturer's instructions (Jiancheng Bioengineering Institute, Nanjing, China). Liver homogenate was prepared by mixing liver tissue with anhydrous ethanol in a 1:9 ratio (1 g liver to 9 mL ethanol), followed by centrifugation at 2000 rpm, 4°C for 10 min to obtain the supernatant. The hepatic TG was measured using lipid assay kit as described above.

2.5. ELISA Analysis of Insulin Levels. The insulin concentration in serum samples was determined using an ELISA kit (Jiangsu Meimian Industrial Co., Ltd.) in accordance with the kit instruction. Specifically, 10 μL of standard solution was added to the standard wells, while 10 μL of serum sample was added to the sample wells. Blank wells received 10 μL of standard/sample diluent. Each well was then supplemented with 100 μL of enzyme-conjugated antibody. The plate was gently mixed, sealed, and incubated at room temperature for 120 min. After incubation, the wells were washed five times with 300 μL of wash buffer. Next, 100 μL of TMB substrate was added to each well, and the plate was incubated in the dark for 30 min to allow color development. The reaction was stopped by adding 50 μL of stop solution to each well. Finally, the optical density (OD) was measured at 450 nm with a reference wavelength of 630 nm using a microplate reader.

2.6. Histomorphological Analysis. Liver, pancreas, and colon tissues preserved in 4% PFA (Solarbio, China) were subjected to hematoxylin and eosin (H&E) staining. After fixation for 24 h, the tissues were dehydrated through a graded series of ethanol concentrations and then cleared with xylene. Subsequently, the tissue samples were fully infiltrated and embedded in paraffin at 60°C. Once cooled, 4 μm thick sections were prepared using a microtome and mounted evenly onto pretreated slides. The slides were then dried at 60°C for at least 1 h. The resulting sections were stained with H&E, followed by microscopic examination.

2.7. RNA Extraction and cDNA Synthesis and Quantitative Real-Time PCR (RT-qPCR). Total RNA was extracted from mouse liver tissues using the TransZol Up Plus RNA Kit (ER501, TransGen Biotech, Beijing, China) according to the manufacturer's protocol with minor modifications. Briefly, approximately 50 mg of liver tissue was homogenized in 1 mL of TransZol reagent using a sterile RNase-free homogenizer. After phase separation with chloroform and subsequent centrifugation at 12,000 × g for 10 min at 4°C, the aqueous phase was collected and mixed with an equal volume of isopropanol. The RNA pellet was obtained by centrifugation, washed with 75% ethanol, and air-dried before resuspension in RNase-free water. RNA purity and concentration were assessed spectrophotometrically using a NanoDrop 2000 (Thermo Fisher Scientific, USA), and integrity was confirmed via 1% agarose gel electrophoresis. Only RNA samples with A260/A280 ratios between 1.8 and 2.1 were used for subsequent reverse transcription.

Reverse transcription was performed using the 5 × All-In-One RT MasterMix (ABM, Canada) in a 20 μL reaction volume containing 1 μg of total RNA, following the manufacturer's instructions. The resulting cDNA was diluted 5-fold and used as the template for RT-qPCR analysis. Quantitative PCR was carried out using the EvaGreen 2 × qPCR MasterMix (ABM, Canada) on a LightCycler 96 system (Roche, Switzerland). Each 20 μL PCR reaction contained 10 μL of 2 × MasterMix, 0.5 μL each of forward and reverse primers (10 μM), 2 μL of cDNA template, and 7 μL of nuclease-free water. Thermal cycling conditions were as follows: initial denaturation at 95°C for 10 min, followed by 40 cycles of 95°C for 15 s and 60°C for 30 s. Melting curve analysis was performed to verify amplification specificity. Gene expression levels were normalized to GAPDH and calculated using the $2^{-\Delta\Delta Ct}$ method. Primer sequences are listed in Table S1.

2.8. Full-Length 16S rRNA Sequencing. Fecal DNA was extracted following methods described in previous studies [21]. The V1–V9 regions of the 16S rRNA gene were amplified by PCR using primers 27F (5′-AGRGTTYGATYMTGGCTCAG-3′) and 1492R (5′-RGYTACCTTGTTACGACTT-3′). The PCR products were assessed by 2% agarose gel electrophoresis, extracted according to the manufacturer's instructions (Pacific Biosciences), and used to construct a SMRTbell library for sequencing via blunt-end ligation. All amplicon sequencing was performed by Shanghai Biozeron Biotechnology Co., Ltd. (Shanghai, China). The resulting FASTA sequences underwent rigorous quality control and alignment, generating an OTU table based on a 97% similarity threshold. Subsequent statistical analyses of bacterial relative abundance and α and β diversities were conducted using R software (version 4.2.3).

2.9. Statistical Analysis. All statistical evaluations were conducted using GraphPad Prism 9 (GraphPad, San Diego, CA). Data were analyzed using one-way analysis of variance (ANOVA) and expressed as mean ± SEM. A p-value of less than 0.05 was considered statistically significant. The group allocation was known to the experimenter who administered the treatments. The experimenters conducting the measurements and the outcome assessments were blinded to the group allocation. Data analysis was performed by a researcher who was also blinded to the group assignments.

3. Results

3.1. Phytochemical Characterization of FTM Extract by UPLC-QTOF-MS. To characterize the principal constituents of the Fritillaria thunbergii aqueous extract, UPLC-QTOF-MS analysis was conducted in positive ion mode. The total ion chromatogram (TIC) (Figure 1) revealed multiple prominent peaks within the retention window of 3–10 min. Eight major compounds were identified based on accurate m/z values, retention times, and MS/MS fragmentation patterns (Figure S1; Table 1), including peimisine-3-β-D-glucoside, puqietinonoside, peimisine, peimine, peiminine, puqiedine, isoverticine, and ebeiedinone. All identified peaks exhibited mass errors within acceptable limits and showed characteristic fragment ions supporting their identities.

To further verify structural assignments, MS/MS spectra of each compound were compared with their corresponding molecular structures (Figure S2). Diagnostic fragmentation patterns were observed, such as neutral loss of glucose residues (162 Da) in glycosidic alkaloids and key fragment ions at m/z 98.0956 and 114.0912 for cevanine-type steroidal alkaloids like peimine and peimisine. These matched fragmentation behaviors provided structural validation consistent with prior reports and affirmed the alkaloid composition of the extract.

3.2. FTM Extract Mitigates HSFD-Induced Obesity and Liver Hypertrophy in Mice. After 7 weeks of HSFD induction, mice in the HSFD group exhibited a significant increase in body weight and epididymal fat mass as compared to those in the ND group ($p < 0.001$) (Figures 2(a), 2(b), 2(d)). Meanwhile, HSFD resulted in the elevation of liver index, although there were no significant changes in the spleen and kidney indices (Figure 2(c)). FTM-L treatment showed no significant effect, but FTM-H led to a notable reduction in body weight ($p < 0.05$) and was close to the ND group. Furthermore, HSFD-caused liver hypertrophy was significantly alleviated following FTM-H intervention ($p < 0.001$) (Figure 2(c)). These findings reveal the favorable effect of FMT on the abnormal glycolipid metabolism-driven phenotype.

3.3. FTM Extract Ameliorates HSFD-Induced Glucose Metabolism Disorders and Pancreatic Damage in Mice. After 7 weeks of HSFD induction, the HSFD group exhibited significant glucose metabolism abnormalities compared to the ND group, including elevated FBG levels (Figure 3(a)), reduced fasting serum insulin (FINS) levels (Figure 2(b)), increased insulin resistance (HOMA-IR, Figure 3(c)), and impaired β-cell function (HOMA-β, Figure 3(d)). FTM-H treatment significantly lowered FBG, restored FINS levels,

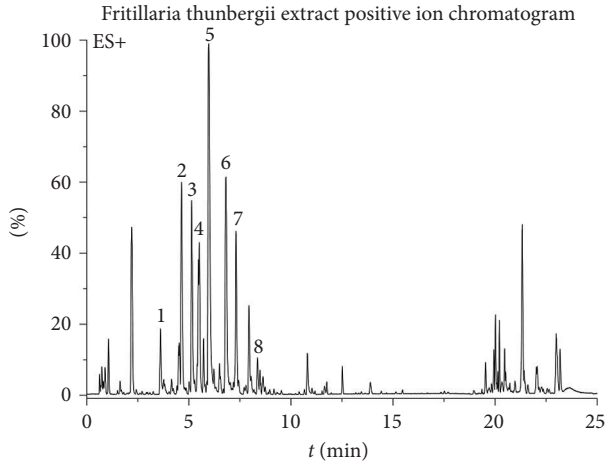


Figure 1: UPLC-QTOF-MS total ion chromatogram (TIC) of *Fritillaria thunbergii* aqueous extract in positive ion mode. Eight major peaks (labeled 1–8) were detected within 3–10 min under optimized UPLC conditions and subjected to MS/MS analysis for structural identification. Peak assignments correspond to representative steroidal alkaloids, including peimisine-3-β-D-glucoside (1), puqietinonoside (2), peimisine (3), peimine (4), peiminine (5), puqiedine (6), isoverticine (7), and ebeiedinone (8).

and improved insulin resistance and β-cell dysfunction in a dose-dependent manner (Figures 3(a), 3(b), 3(c), 3(d)). Histopathological analysis further revealed that the ND group displayed intact islet structures, while the HSFD group showed a disrupted islet architecture, β-cell atrophy, and inflammatory infiltration (Figures 3(e), 3(f), 3(g)). FTM-H treatment preserved islet morphology and reduced inflammation, whereas FTM-L treatment provided only partial protection. These findings suggest that FTM extract mitigates HSFD-induced glucose metabolism disorders and pancreatic damage, highlighting its potential as a therapeutic agent for metabolic diseases.

3.4. FTM Extract Attenuates HSFD-Induced Lipid Metabolism Disorders and Hepatic Steatosis in Mice. After 7 weeks of HSFD induction, mice in the HSFD group demonstrated significant disruptions in lipid metabolism compared to those in the ND group, including markedly elevated levels of TC, TG, and LDL-c in both serum and liver ($p < 0.001$, Figures 4(a), 4(b), 4(c), 4(d), 4(e)). Treatment with FTM, particularly at FTM-H, significantly reduced these lipid levels in a dose-dependent manner ($p < 0.001$, Figures 4(a), 4(b), 4(c), 4(d), 4(e)). Concurrently, the HSFD group exhibited an increased liver index (Figure 2(c)), indicative of hepatic steatosis. Histological analysis revealed pronounced lipid vacuole accumulation and nuclear displacement in hepatocytes (Figures 4(f), 4(g), 4(h)). FTM-H treatment effectively ameliorated these pathological changes and restored hepatic structure, whereas FTM-L showed only partial efficacy. These results indicate that FTM extract mitigates HSFD-induced lipid metabolic disturbances and hepatic damage in a dose-dependent manner, underscoring its therapeutic potential for lipid metabolism disorders.

3.5. Hepatic mRNA Expression Patterns in Response to FTMH Treatment. RT-qPCR analysis (Figure 5) demonstrated that HSFD caused widespread transcriptional disruption in hepatic metabolic and immune signaling networks, with FTMH inducing targeted and directionally consistent regulatory effects. A marked increase in PI3K expression was observed in the HSFD group, which was further elevated following FTMH administration. Although IRS1 and IRS2 did not exhibit significant suppression under HSFD, both were significantly upregulated after treatment, indicating a recovery of key insulin signaling components. In parallel, GLUT1 was significantly elevated in the HSFD group and effectively suppressed by FTMH, suggesting attenuation of HSFD-induced dysregulation in glucose transport.

The hepatic lipogenic program was strongly activated by HSFD, as evidenced by significant upregulation of ACC1, SCD1, and FAS, while SREBP1 remained statistically unchanged. Among these, FTMH selectively suppressed SCD1 and SREBP1, with ACC1 and FAS showing downward trends without reaching significance. In contrast, genes involved in lipid oxidation and trafficking were largely unresponsive to HSFD but showed consistent induction after FTMH intervention. Notably, PPARα and LDLR, which remained stable under HSFD conditions, were both significantly upregulated following treatment. PGC-1α and FXR, already increased under HSFD, were further enhanced by FTMH. MCAD also displayed a treatment-specific increase, reinforcing the pattern of enhanced oxidative lipid processing.

HSFD also induced a strong proinflammatory signature, reflected by significant increases in IL-1β, IL-6, NF-κB, and IKK2. Among these, FTMH significantly suppressed NF-κB and IKK2, while IL-1β and IL-6 showed modest reductions that did not achieve statistical significance. The anti-inflammatory cytokine IL-10, which was significantly downregulated by HSFD, was strongly restored and even exceeded baseline levels following treatment. Furthermore, Myd88 and NCF2, both reduced in the HSFD group, were significantly upregulated by FTMH. Although FOXp3 expression remained stable under HSFD conditions, it exhibited a significant increase after treatment. The expression of TLR4, CD14, CD206, and NCF1 was not significantly altered among groups, and CD36 remained elevated following intervention.

In genes associated with oxidative defense and mitochondrial regulation, SOD1 showed a progressive and significant increase from NC to HSFD and further to FTMH. SOD2 was significantly elevated by HSFD but remained unchanged after treatment. While GPX1, GPX3, GSR, and FXR were induced under HSFD and maintained at comparable levels post-treatment, GPX2, unchanged under HSFD, was significantly increased only in the FTMH group. nNOS and CD86 also demonstrated significant induction after treatment, while CAT and SIRT1 remained stable across all groups. These findings collectively indicate that FTMH exerted structured regulatory effects on metabolic and immune gene expression, including both statistically significant changes and coordinated transcriptional shifts, particularly

Table 1: Identification of major chemical compounds from *Fritillaria thunbergii* by UPLC-QTOF-MS.

Number	Compounds	Retention time (min)	Measured value (m/z)	Calculated value (m/z)	Error (ppm)	Formula	Ion mode	Major fragment (m/z)
1	Peimisine-3-β-D-glucoside	3.62	590.3699	590.3693	1.0	$C_{33}H_{52}NO_8$	Positive	114.0900, 572.3592, 84.0840
2	Puqietinonoside	4.64	592.3864	592.3849	2.5	$C_{34}H_{57}NO_7$	Positive	574.3793, 592.3921, 412.3234, 394.3118
3	Peimisine	5.14	428.3188	428.3165	5.4	$C_{27}H_{41}NO_3$	Positive	428.3266, 114.0920, 109.1019, 126.1297, 84.0822
4	Peimine	5.51	432.3495	432.3478	3.9	$C_{27}H_{45}NO_3$	Positive	414.3432, 432.3556, 398.3112, 112.1121, 98.0956
5	Peiminine	5.98	430.3398	430.3321	17.9	$C_{27}H_{43}NO_3$	Positive	412.3378, 430.3496, 396.2924, 98.0972
6	Puqiedine	6.82	416.3561	416.3529	7.7	$C_{27}H_{45}NO_2$	Positive	98.0976, 145.0947
7	Isoverticine	7.31	432.3489	432.3478	2.5	$C_{27}H_{45}NO_3$	Positive	432.3542, 414.3423, 398.3076
8	Ebeiedinone	8.36	414.3369	414.3372	−0.7	$C_{27}H_{43}NO_2$	Positive	414.3398, 415.3423, 98.0866, 105.0743

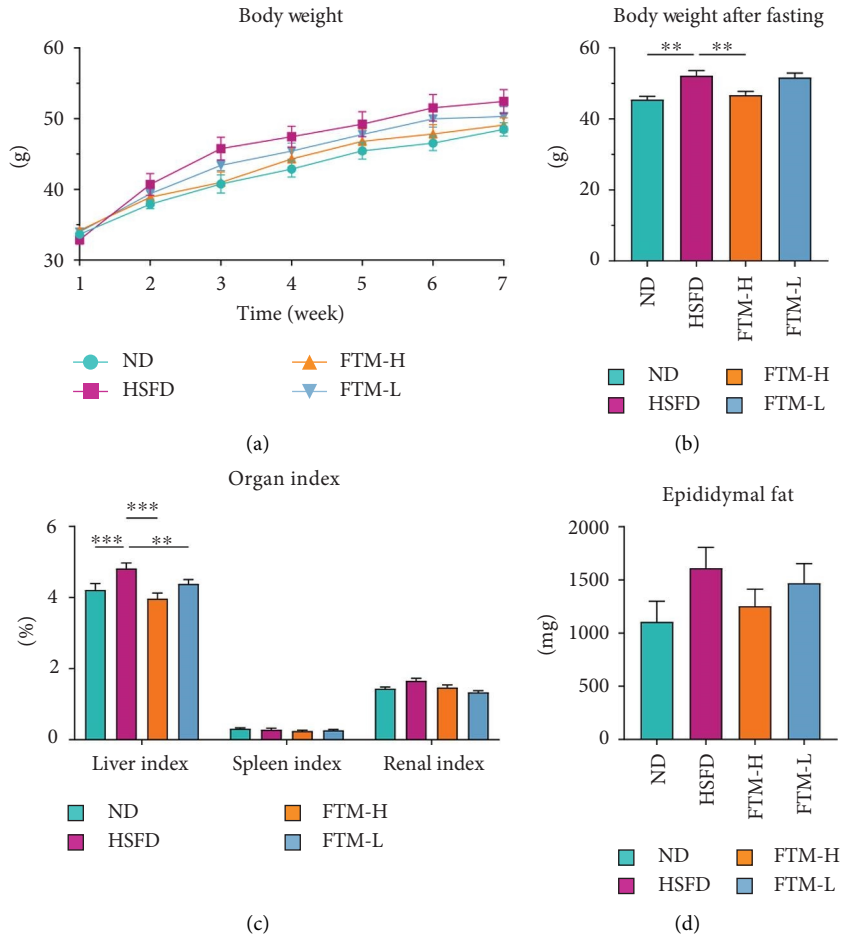


Figure 2: Effects of FTM on body weight, organ indices, and epididymal fat in mice under different dietary conditions. (a) Time-course changes in body weight over 7 weeks among the ND, HSFD, FTM-H, and FTM-L groups. (b) Fasting body weight before tissue collection, demonstrating the impact of high-fat diet and FTM treatment. (c) Organ indices for liver, spleen, and kidney, represented as percentages of organ weight relative to body weight; significant differences were observed in the liver index. (d) Epididymal fat weight, showing variations across experimental groups. Data are presented as mean ± SEM, with significant differences indicated by $^{**}p < 0.01$ and $^{***}p < 0.001$. ND, normal diet; HSFD, high-sugar and high-fat diet; FTM-H, high-dose FTM; FTM-L, low-dose FTM.

in pathways governing lipogenesis, inflammation, and redox balance.

3.6. Protective Effects of FTM Aqueous Extract Against HSFD-Induced Colonic Injury in Mice. H&E-stained colon sections (Figures 6(a), 6(b), 6(c)) revealed pronounced structural abnormalities in HSFD-treated mice, including disrupted crypt architecture, goblet cell atrophy, and significant inflammatory cell infiltration. These findings indicate that HSFD not only impairs metabolic functions but also compromises colonic tissue integrity. Notably, treatment with the aqueous extract of FTM exhibited protective effects. FTM-treated mice displayed largely preserved crypt morphology, an abundance of mucus-filled goblet cells, and reduced inflammatory infiltration compared to the HSFD group. These protective effects were dose-dependent, with higher doses of FTM providing greater mitigation of HSFD-induced colonic injury and inflammation. To investigate the regulatory mechanisms of FTM on gut health, 16S rRNA sequencing was performed to assess its impact on microbiota composition, with the aim of elucidating potential associations between FTM treatment, specific microbial taxa, and HSFD-induced glucose–lipid dysregulation.

3.7. FTM Extract Modulates Gut Microbiota Composition in HSFD-Treated Mice. 16S rRNA sequencing was utilized to analyze bacterial communities in fecal samples, with α-diversity measured using the Shannon, Simpson, and Chao1 indices (Figures 7(a), 7(b), 7(c)). The results demonstrated no statistically significant differences in α-diversity among groups, indicating that FTM treatment did not markedly alter microbial richness or evenness. To further investigate the impact of FTM on gut microbiota structure, PCA, NMDS, and PLS-DA analyses were conducted (Figures 7(d), 7(e), 7(f)). HSFD administration resulted in distinct shifts in microbial composition along the PCA1 and NMDS1 axes, reflecting significant structural changes. High-dose FTM treatment modulated these alterations, suggesting a regulatory effect on gut microbiota structure.

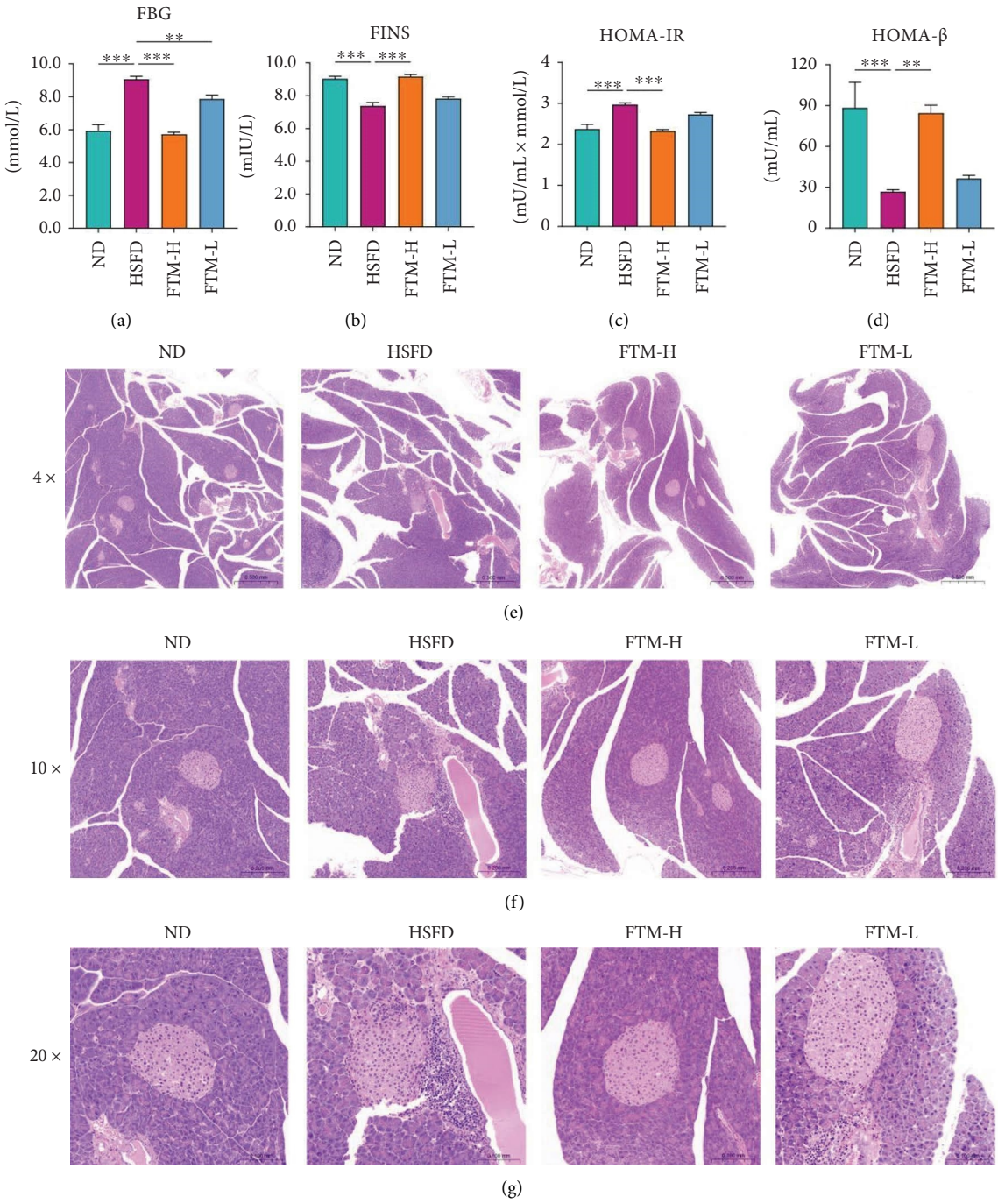


Figure 3: FTM on glucose metabolism and pancreatic histology in mice. (a–d) Biochemical parameters related to glucose metabolism: (a) fasting blood glucose (FBG, mmol/L), (b) fasting insulin (FINS, mIU/L), (c) homeostasis model assessment of insulin resistance (HOMA-IR), and (d) homeostasis model assessment of beta-cell function (HOMA-β). Data are expressed as mean ± SEM, with significant differences indicated by $^{**}p < 0.01$ and $^{***}p < 0.001$. (e–g) Pancreatic tissues stained with H&E, showing the morphology of islets across experimental groups: ND, HSFD, FTM-H, and FTM-L, from left to right. Scale bars = 0.5 mm (e), 0.2 mm (f), and 0.1 mm (g). Changes in islet size, architecture, and cellular distribution are evident in different dietary and treatment conditions.

At the phylum level, Firmicutes, Bacteroidota, Desulfobacterota, Verrucomicrobiota, Patescibacteria, and Campilobacterota constituted the dominant phyla, collectively accounting for over 90% of total abundance. High-dose FTM treatment significantly increased the relative abundances of Firmicutes and Desulfobacterota while reducing those of Bacteroidota, Verrucomicrobiota, Campilobacterota, and Patescibacteria (Figure 7(g)). At the genus level, HSFD feeding was associated with increased abundances of *Akkermansia* and *Allobaculum*, alongside a reduction in *Lachnospiraceae NK4A136 group*, *Lactobacillus*, *Faecalibaculum*, and *Desulfovibrio*. High-dose FTM treatment

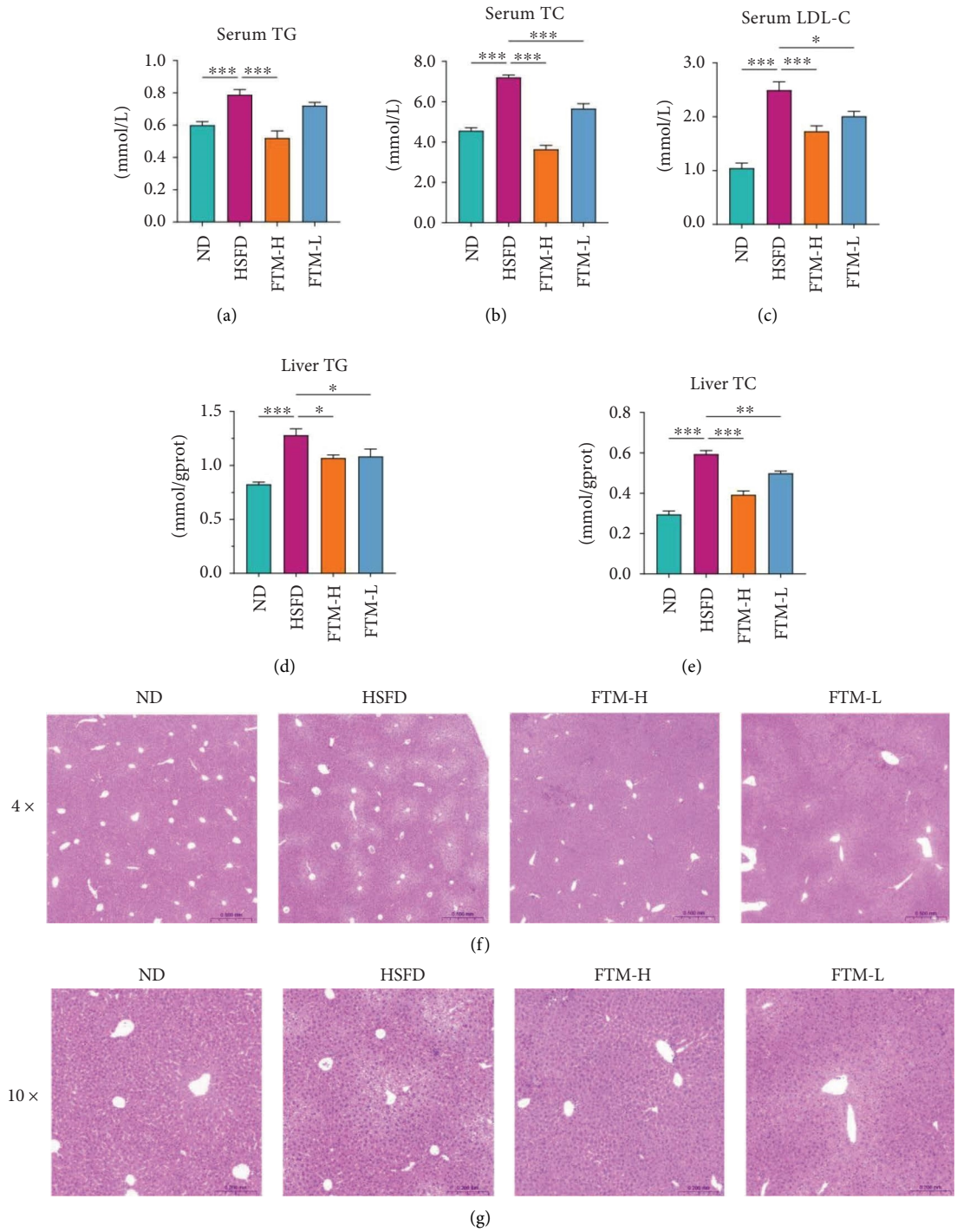


Figure 4: Continued.

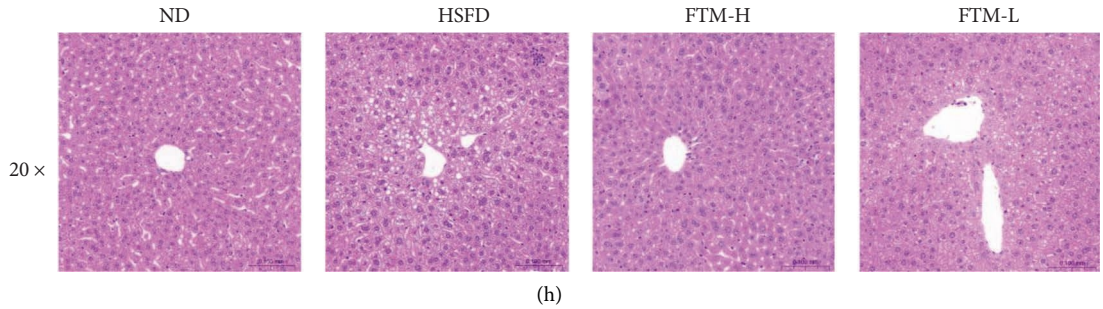


Figure 4: Effects of FTM on lipid metabolism and liver histology in mice under different dietary conditions. (a–e) Lipid profiles in serum and liver: (a) serum triglycerides (TG, mmol/L), (b) serum total cholesterol (TC, mmol/L), (c) serum low-density lipoprotein cholesterol (LDL-c, mmol/L), (d) liver triglycerides (TG, mmol/g prot), and (e) liver total cholesterol (TC, mmol/g prot). Data are expressed as mean ± SEM. Statistical significance was analyzed using one-way ANOVA, with $^{*}p < 0.05$, $^{**}p < 0.01$, and $^{***}p < 0.001$ indicating significance. (f–h) H&E-stained liver sections illustrating histological changes across dietary and treatment groups: ND, HSFD, FTM-H, and FTM-L, from left to right. Images highlight structural alterations such as hepatocyte morphology and lipid droplet deposition at three magnifications (f: 0.5 mm; g: 0.2 mm; h: 0.1 mm). Scale bars are provided for each magnification. Treatment with FTM reduces lipid accumulation and improves hepatocyte integrity compared to the HSFD group, demonstrating its potential hepatoprotective effects.

reversed these changes by upregulating *Lachnospiraceae NK4A136 group*, *Faecalibaculum*, *Desulfovibrio*, and *Blautia* while downregulating *Lactobacillus*, *Akkermansia*, and *Allobaculum* (Figure 7(h)). These findings underscore the capacity of FTM to modulate gut microbiota composition in a dose-dependent manner, highlighting its potential role in ameliorating HSFD-induced metabolic disturbances.

3.8. FTM Intervention Mitigates HSFD-Induced Gut Dysbiosis by Enhancing Beneficial Taxa. LEfSe analysis demonstrated that FTM intervention significantly counteracted HSFD-induced gut dysbiosis by enriching specific taxa associated with beneficial metabolic functions (Figures 8(a), 8(b)). The cladogram (Figure 8(a)) highlighted the increased abundance of *Firmicutes*, *Lachnospiraceae*, *Oscillospiraceae*, and *Clostridium* in the FTM-treated group, taxa linked to SCFA production and carbohydrate metabolism (Figure 8(b)). Furthermore, the enrichment of *Romboutsia* in the FTM group suggests improvements in gut barrier integrity and anti-inflammatory responses, highlighting FTM's protective role in maintaining gut health. In contrast, HSFD feeding promoted *Akkermansia* and *Verrucomicrobiota*, taxa associated with elevated gut permeability and metabolic disturbances. Notably, although *Akkermansia* has beneficial effects under normal conditions, its overgrowth in HSFD-induced dysbiosis may contribute to further metabolic disruption. The LDA plot (Figure 8(b)) further quantified intergroup differences, showing that the FTM group harbored taxa actively involved in carbohydrate, amino acid, and lipid metabolism. These taxa likely support the production of SCFAs, amino acids, and anti-inflammatory metabolites, contributing to improved gut health and metabolic regulation. Collectively, these findings indicate that FTM promotes the restoration of gut homeostasis and mitigates HSFD-induced dysbiosis by reorganizing microbial networks and enhancing beneficial metabolic activities.

3.9. FTM Extract Alleviates HSFD-Induced Metabolic Dysfunction by Modulating Gut Microbiota Composition and Functional Pathways. PICRUSt2 analysis was employed to predict the functional potential of the gut microbiota across the three experimental groups. The HSFD group exhibited significant metabolic disruption, characterized by elevated activity in pathways related to carbohydrate metabolism, amino acid metabolism, and secondary metabolite synthesis (Figures 9(c), 9(e)). These metabolic changes were strongly associated with dysregulated energy metabolism and the development of metabolic disorders. In contrast, the ND group maintained stable pathway activity across all examined categories (Figures 9(a), 9(c), 9(e)). Notably, the FTM-treated group displayed metabolic profiles resembling those of the ND group, reflecting the regulatory effects of FTM on HSFD-induced metabolic imbalance. Specifically, FTM treatment significantly reduced the overactivation of carbohydrate (Figures 9(c), 9(d)) and amino acid metabolism pathways (Figures 9(e), 9(f)) observed in the HSFD group while moderately upregulating pathways related to ABC transporters and secondary metabolite synthesis (Figures 9(e), 9(f)). These findings suggest that FTM exerts its therapeutic potential through multilayered modulation of metabolic networks, alleviating metabolic disturbances induced by HSFD.

Further, the Spearman correlation analysis (Figure 10(a)) demonstrated significant relationships between gut microbiota and metabolic markers. Beneficial taxa such as *Lachnoclostridium*, *Lachnospiraceae UCG-006*, *Romboutsia*, and *Lachnospiraceae bacterium* were negatively correlated with metabolic markers such as TC, TG, and LDL-C, indicating their contribution to metabolic improvement. In contrast, *Akkermansia* showed a positive correlation with metabolic markers, suggesting its potential role in HSFD-induced metabolic imbalance. Relative abundance analysis (Figures 10(b), 10(c), 10(d), 10(e), 10(f), 10(g), 10(h)) revealed that beneficial taxa, including *Lachnoclostridium* and *Lachnospiraceae UCG-006*, were significantly enriched in the FTM-treated group compared to those in the HSFD group. Similarly, *Romboutsia* and *Lachnospiraceae bacterium* exhibited higher abundance in the FTM

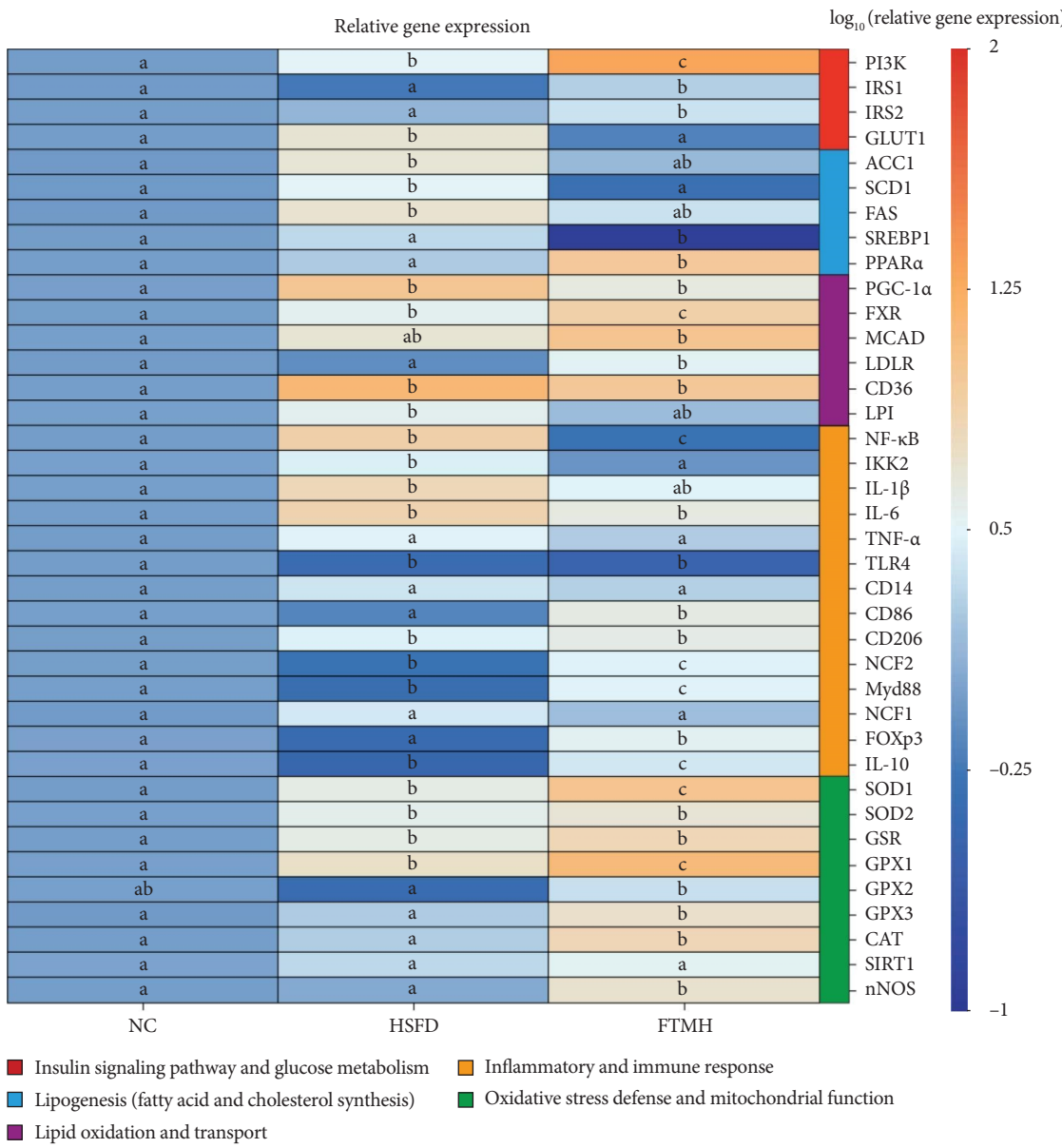


Figure 5: Transcriptomic profiling of hepatic genes involved in insulin signaling and glucose metabolism, lipogenesis, lipid oxidation and transport, inflammatory and immune response, and oxidative stress defense and mitochondrial function. Heatmap of hepatic gene expression levels across groups. Relative mRNA expression of 38 genes was assessed by RT-qPCR, and log10-transformed values were used for visualization. Genes were selected to represent key pathways involved in insulin signaling and glucose metabolism (red), lipogenesis (fatty acid and cholesterol synthesis) (blue), lipid oxidation and transport (purple), inflammatory and immune response (yellow), and oxidative stress defense and mitochondrial function (green). The color scale indicates log10(relative expression), with red representing upregulation and blue representing downregulation. Statistical grouping is indicated by letters (a, b, c); bars sharing the same letter are not significantly different ($p > 0.05$), as determined by one-way ANOVA followed by Tukey's post hoc test. Abbreviations: NC, normal control; HSFD, high-sugar high-fat diet; FTMH, Fritillaria thunbergii Miq. extract-treated group.

group, whereas *Akkermansia* and *Clostridium* sp. remained low in abundance. These results underscore FTM's ability to regulate gut microbiota composition, suppress harmful taxa, and enrich beneficial microbes, ultimately mitigating HSFD-induced metabolic dysregulation. Collectively, the findings highlight the critical role of gut microbiota in metabolic regulation and emphasize FTM's therapeutic potential for metabolic disorders.

4. Discussion

This study demonstrates that FTM aqueous extract has significant potential in alleviating metabolic disorders induced by a HSFD. Our findings highlight its dual functionality as a nutritional and bioactive resource, positioning it as a promising candidate for developing functional food products aimed at improving metabolic health.

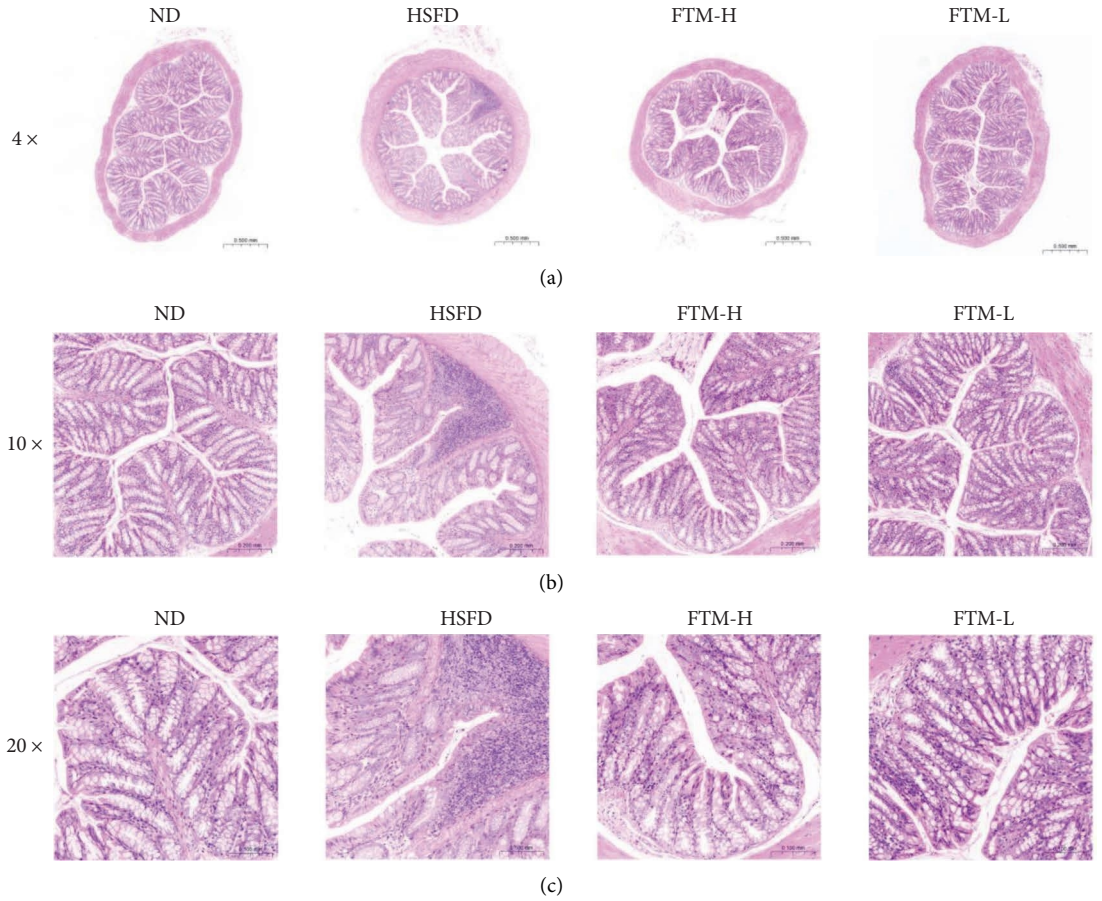


Figure 6: Effects of FTM on intestinal morphology in mice under different dietary conditions. (a–d) H&E-stained sections of mouse intestines at three magnifications (a: 0.5 mm, b: 0.2 mm, c: 0.1 mm) across experimental groups: ND, HSFD, FTM-H, and FTM-L, from left to right. The histological images illustrate villus architecture, crypt depth, and overall structural integrity of the intestinal mucosa. The HSFD group exhibited noticeable disruptions, including shortened villi and increased crypt depth, indicative of intestinal injury. FTM treatment, particularly at a high dose, demonstrated a protective effect, with improved villus height and crypt organization, suggesting restoration of intestinal structure. Scale bars are provided for each magnification to ensure accurate visualization.

The data presented herein demonstrate that FTM significantly attenuates obesity and hepatic steatosis, as evidenced by a reduction in body weight and liver hypertrophy. Specifically, high-dose FTM (1.3 g/kg) treatment led to a marked decrease in body weight, bringing levels closer to those observed in the ND group. Moreover, FTM-H treatment reversed the increase in liver index induced by the HSFD. The reduction in body weight and hepatic hypertrophy following FTM treatment suggests that this intervention mitigates the metabolic disturbances caused by a high-fat diet. This is particularly significant, as obesity and nonalcoholic fatty liver are important components of glycolipid metabolism disorders and are closely linked to dysregulated lipid metabolism [22, 23]. The observed effects of FTM in reducing lipid accumulation in the liver and improving metabolic function are likely due to its ability to modulate systemic inflammation and lipid processing pathways [24, 25], as has been demonstrated for other plant-based therapeutic agents.

In addition to its effects on lipid metabolism, FTM treatment also yielded significant improvements in glucose metabolism. Specifically, FTM-H treatment reduced FBG levels and improved insulin sensitivity, as indicated by lower HOMA-IR scores and restored β-cell function. These results indicate that FTM not only alleviates obesity-related metabolic dysfunction but also directly contributes to the regulation of glucose homeostasis. Histological analyses corroborated these findings, as FTM treatment preserved pancreatic islet integrity and reduced inflammatory infiltration in the pancreas. In contrast, the HSFD group exhibited significant β-cell atrophy and pancreatic inflammation, which are indicative of impaired pancreatic function. These results suggest that FTM exerts protective effects on pancreatic tissue and may contribute to the restoration of β-cell function and improved insulin sensitivity.

The broad-spectrum regulation of hepatic gene expression observed following FTMH treatment reflects a multitargeted mechanism of action consistent with the complex pathophysiology of metabolic disorders. In particular, among lipogenic genes, SREBP1 and SCD1 were significantly suppressed by FTMH, whereas ACC1 and FAS exhibited only downward trends without reaching statistical

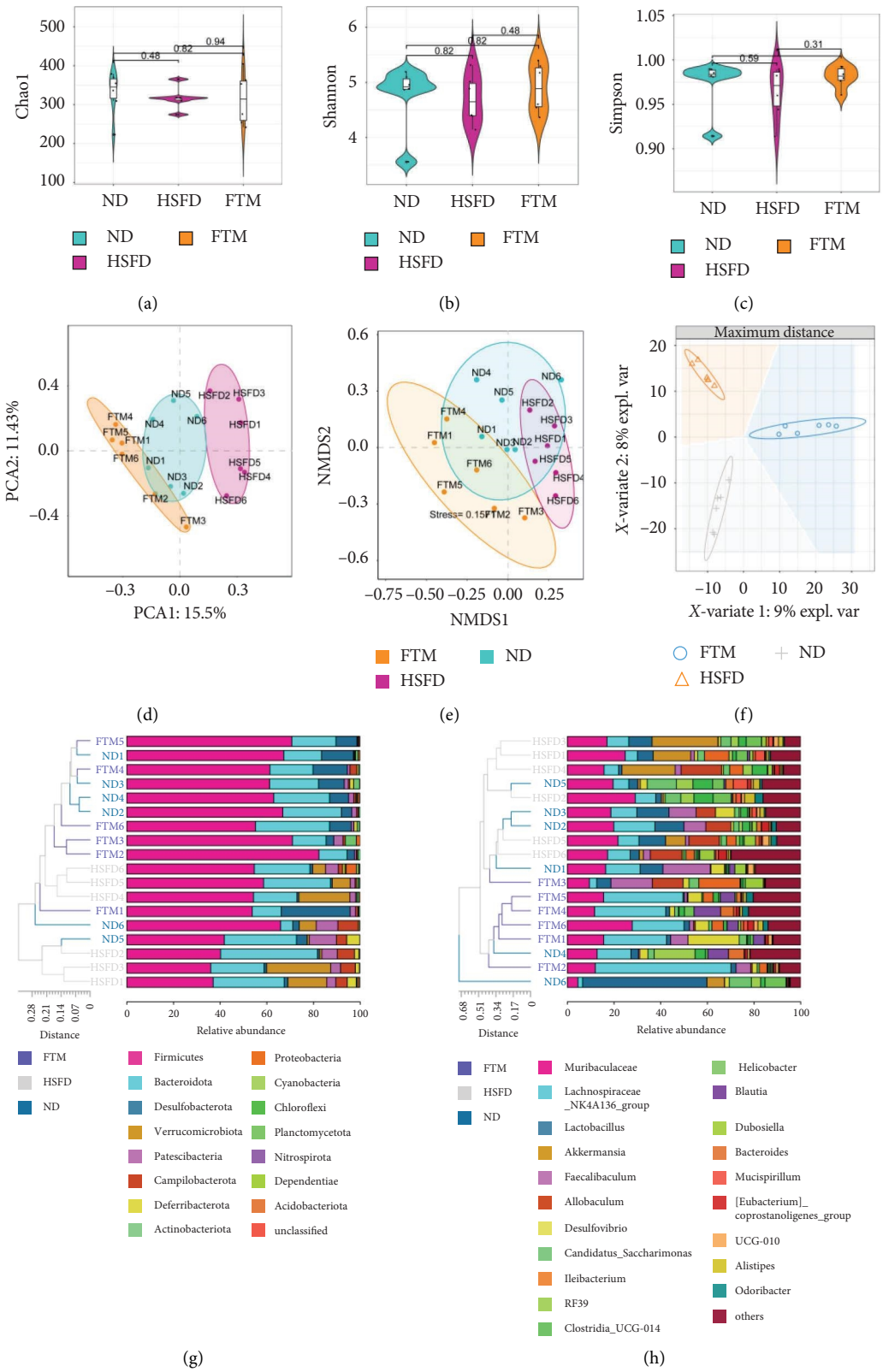


FIGURE 7: Effects of Fritillaria thunbergii (FTM) on gut microbiota composition and diversity under different dietary conditions. (a–c) Alpha diversity indices of gut microbiota, including (a) observed OTUs, (b) Shannon index, and (c) Simpson index, illustrating microbial richness and evenness across ND, HSFD, and FTM groups. Data are presented as box plots with significant differences denoted ($^{*}p < 0.05$). (d–f) Beta diversity analyses of gut microbial communities: (d) Principal component analysis (PCA), (e) nonmetric multidimensional scaling (NMDS) based on the Bray–Curtis dissimilarity, and (f) partial least-squares discriminant analysis (PLS-DA). Distinct clustering patterns highlight significant differences in microbial composition among the groups, with FTM treatment partially reversing the HSFD-induced dysbiosis. (g–h) Taxonomic composition of gut microbiota: (g) Bar plots representing the relative abundance of bacterial phyla, showing shifts in microbial populations induced by HSFD and subsequent restoration with FTM treatment. (h) Bar plots representing the relative abundance of bacterial genera. The HSFD group exhibited reduced beneficial bacteria, while FTM treatment restored microbial balance toward the ND group profile. Data indicate the modulatory effects of FTM on gut microbiota diversity and composition, potentially mitigating HSFD-induced dysbiosis.

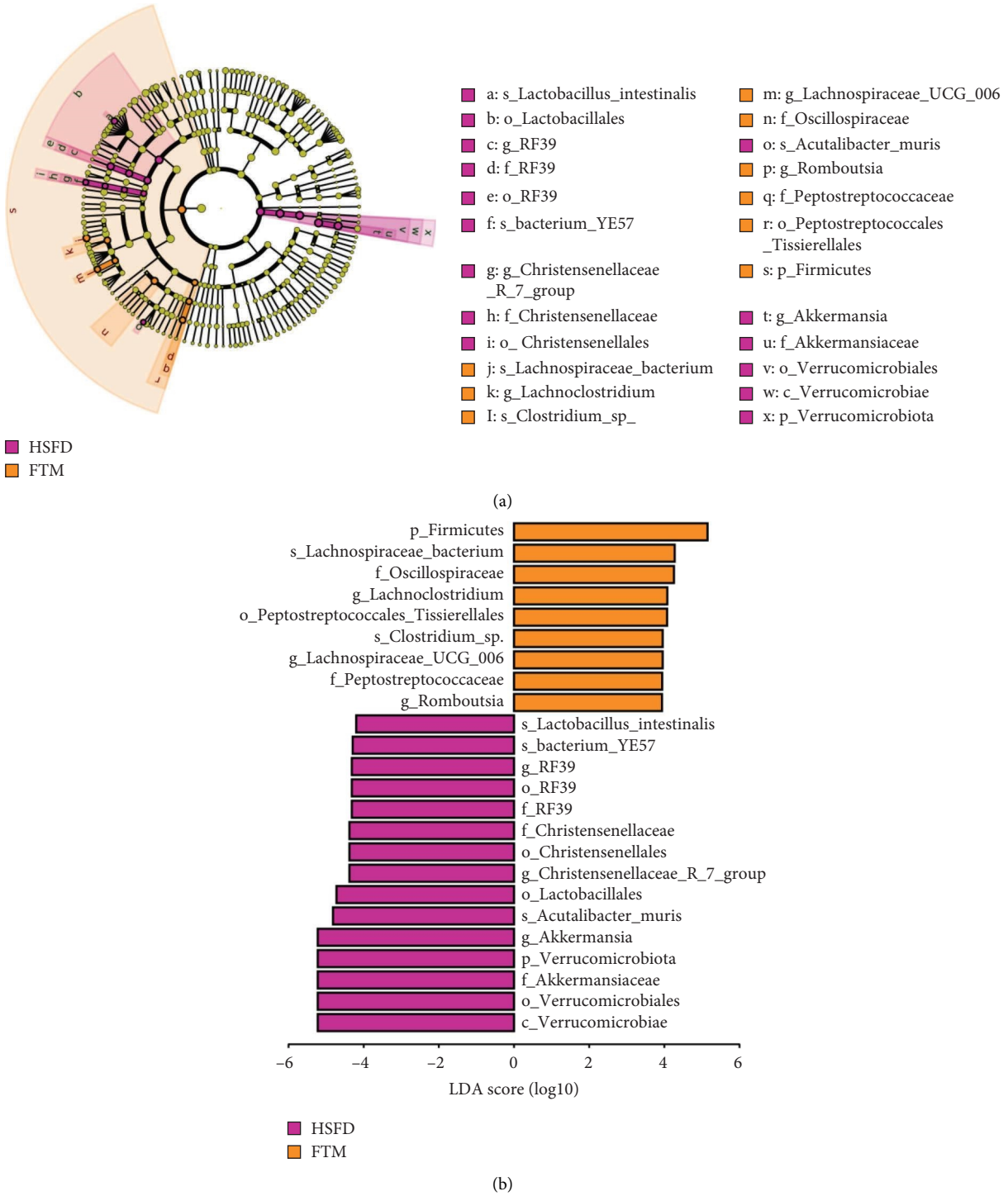


Figure 8: Differential analysis of gut microbiota composition between HSFD and FTM groups. (a) Cladogram generated from LEfSe (linear discriminant analysis effect size) analysis, showing taxonomic differences in the gut microbiota between HSFD and FTM groups. Nodes represent taxonomic levels (from phylum to species), with significantly enriched taxa in HSFD and FTM groups highlighted in purple and orange, respectively. Taxa identified as key contributors to group differences are labeled. (b) Linear discriminant analysis (LDA) scores of differentially abundant taxa between the HSFD and FTM groups. Positive LDA scores (orange bars) indicate taxa enriched in the FTM group, while negative LDA scores (purple bars) represent taxa enriched in the HSFD group. Taxa with LDA scores > 2.0 are considered significant contributors to group differences. These results suggest that FTM treatment modulates gut microbial composition by promoting beneficial taxa (e.g., *Lachnospiraceae* and *Akkermansia*) while reducing harmful bacteria associated with the HSFD group, highlighting its potential role in restoring gut microbiota balance.

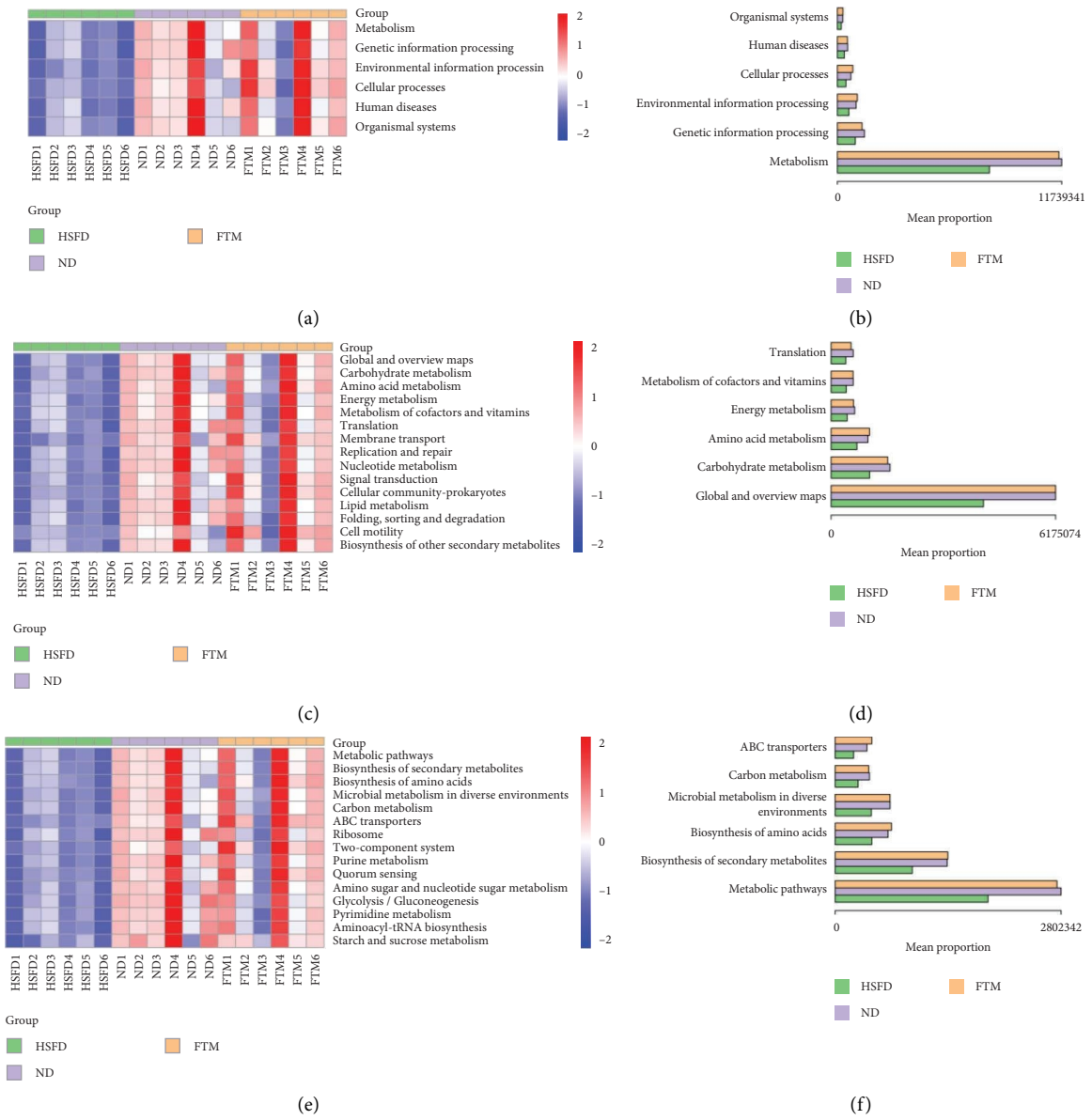


Figure 9: Predictive analysis of PICRUSt2 function in gut microbiota under FTM treatment. KEGG pathway analysis of microbial communities in the HSFD, ND, and FTM groups using PICRUSt2. (a) Heatmap showing the enrichment of microbial pathways across higher-level KEGG functional categories, including metabolism, genetic information processing, environmental information processing, cellular processes, human diseases, and organismal systems. (b) Bar plot depicting the contribution of pathways to the overall functional profile of each group, with a focus on metabolic pathways. (c) Heatmap displaying specific metabolic pathways, including carbohydrate metabolism, amino acid metabolism, energy metabolism, and nucleotide metabolism. (d) Bar plot illustrating the contribution of pathways related to translation, metabolism of cofactors and vitamins, energy metabolism, amino acid metabolism, and carbohydrate metabolism in the different groups. (e) Heatmap of additional metabolic pathways, such as biosynthesis of secondary metabolites, microbial metabolism in diverse environments, and carbon metabolism. (f) Bar plot showing the contribution of key functional categories, including ABC transporters, carbon metabolism, biosynthesis of amino acids, and metabolic pathways across the treatment groups.

significance, indicating inhibition of de novo fatty acid synthesis [26, 27]. This pattern supports the phenotypic improvements in hepatic steatosis and aligns with prior evidence suggesting that attenuation of SREBP1-driven lipogenic pathways can ameliorate lipid overload in diet-induced models of NAFLD and metabolic syndrome [28, 29]. Furthermore, the upregulation of lipid uptake and transport-related genes such as LDLR [30, 31] and LPI [32] suggests enhanced hepatic clearance of circulating lipids, potentially contributing to the observed reduction in serum and hepatic triglyceride levels.

FTM also modulated key mediators of glucose metabolism. The restoration of IRS1 expression, coupled with the continued elevation of PGC-1α observed under HSFD conditions, suggests a partial reactivation of hepatic insulin signaling. Both IRS2 and PI3K were significantly

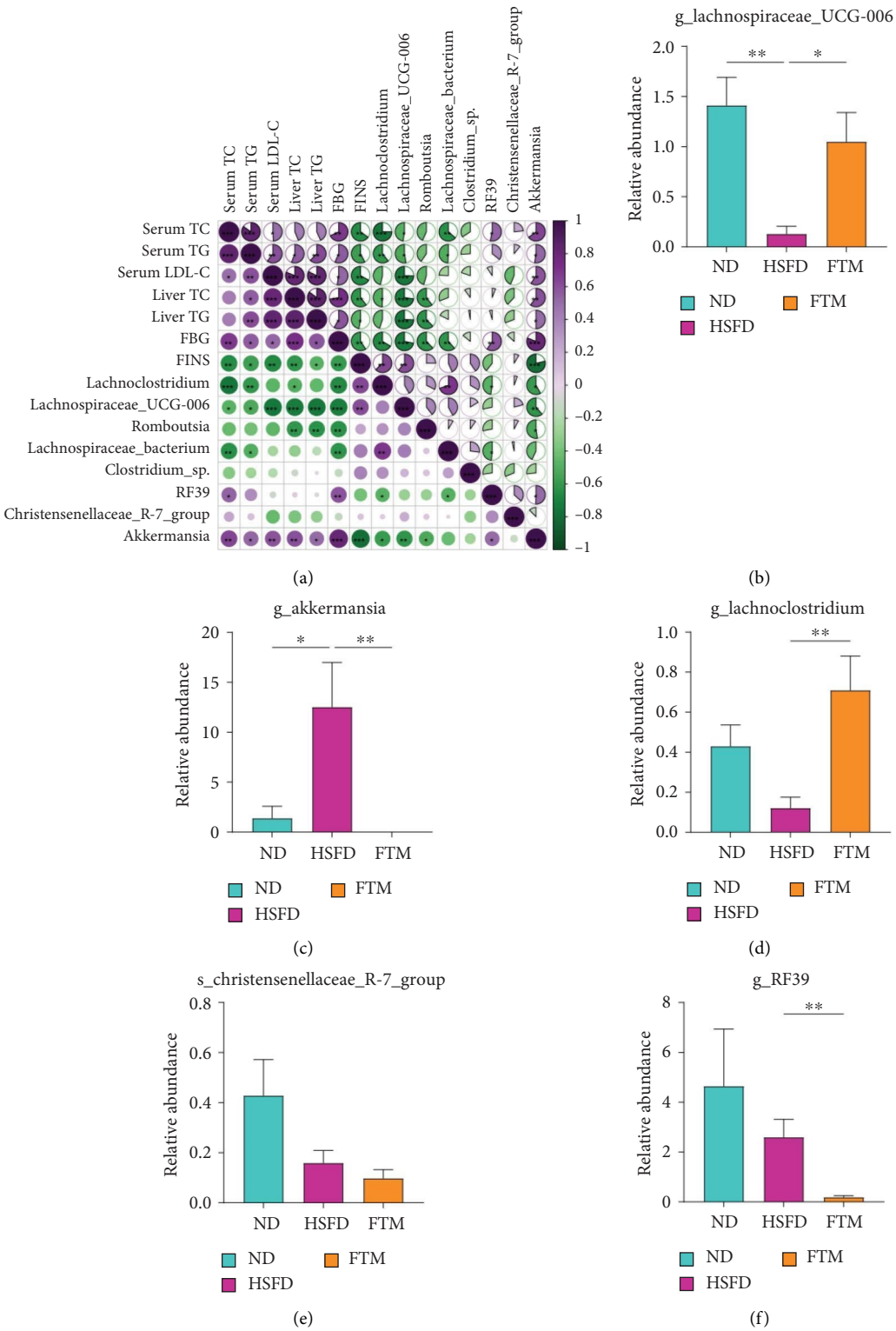


Figure 10: Continued.

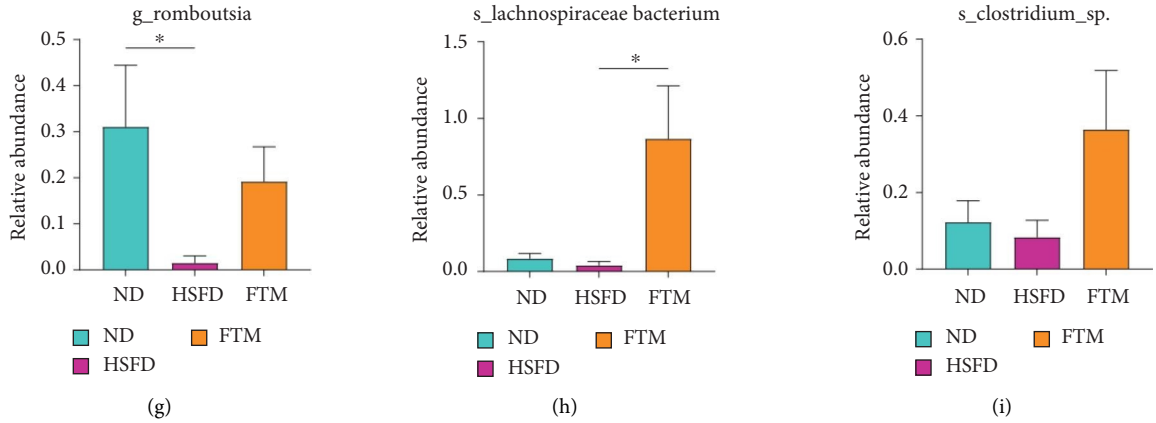


Figure 10: Correlation analysis and relative abundances of gut microbiota under FTM treatment. (a) Correlation matrix of bacterial genera with key physiological and metabolic parameters. Spearman correlation coefficients are visualized using the color intensity and size of circles, with purple indicating positive correlations and green indicating negative correlations. Significant correlations between specific bacterial genera and host metabolic markers underscore the modulatory effects of FTM on host–microbe interactions. (b–i) Relative abundances of key bacterial taxa across experimental groups (ND: normal diet; HSFD: high-sugar and high-fat diet; FTM: *Fritillaria thunbergii* Miq. treatment). Notable bacterial genera include *Lachnospiraceae_UCG-006* (b), *Akkermansia* (c), *Lachnoclostridium* (d), *Christensenellaceae_R-7_group* (e), *RF39* (f), *Romboutsia* (g), *Lachnospiraceae bacterium* (h), and *Clostridium* sp. (i). Bars represent mean ± SEM, and statistical significance is indicated by $^{*}p < 0.05$, $^{**}p < 0.01$, $^{***}p < 0.001$. FTM treatment effectively restores the relative abundances of beneficial bacteria disrupted by HSFD, particularly short-chain fatty acid–producing taxa, supporting its therapeutic potential in mitigating HSFD-induced gut dysbiosis.

upregulated following FTMH treatment. The transcriptional reactivation of PGC-1α may compensate by enhancing mitochondrial biogenesis and promoting metabolic flexibility [33, 34]. These findings point toward FTM's ability to correct diet-induced insulin resistance through upstream and downstream modulations of hepatic insulin pathways.

In terms of immune regulation, FTMH elicited a pronounced shift toward an anti-inflammatory hepatic microenvironment. The NF-κB and IKK2 were significantly suppressed by FTMH, without statistical significance. In contrast, IL-10 was significantly enhanced, while CD206 remained elevated but unchanged compared to HSFD, indicating a transition from M1- to M2-like macrophage phenotypes and suggests suppression of sterile inflammation commonly associated with overnutrition [35–37]. The partial restoration of Myd88 and NCF2 further reflects FTM's modulation of TLR4-dependent innate immune pathways, which have been implicated in hepatic insulin resistance and lipotoxicity [38].

However, FTMH exhibited limited influence on classic antioxidant gene expression. Multiple antioxidant genes, including SOD1, GPX1, GPX3, GSR, and FXR, were significantly elevated in response to HSFD and remained elevated after FTMH treatment, suggesting that the antioxidant effects of FTM may be mediated through direct radical scavenging or nontranscriptional mechanisms [39]. GPX2 was significantly induced by FTMH, while PGC-1α, already elevated under HSFD, showed no further significant change, which may reflect a partial activation of mitochondrial protective responses, but these changes alone are unlikely to fully restore redox homeostasis [40, 41]. Taken together, the transcriptional data suggest that FTM exerts its metabolic benefits by orchestrating coordinated modulation of hepatic lipogenesis, insulin signaling, and inflammatory responses, while its antioxidant effects may rely on alternative pathways not captured at the mRNA level.

A novel and significant finding of this study is the effect of FTM on gut microbiota composition. Dysbiosis, often characterized by an altered gut microbiota profile, is widely recognized as a contributing factor to metabolic diseases, including obesity and insulin resistance. Our data show that FTM treatment, particularly at the high dose, induced significant shifts in microbial composition. Notably, FTM administration increased the relative abundance of beneficial bacteria such as *Lachnospiraceae* and *Faecalibaculum*, while reducing the abundance of potentially pathogenic taxa, including *Akkermansia*.

The enrichment of *Lachnospiraceae* and *Faecalibaculum*, both of which are known to produce SCFAs, underscores FTM's potential to restore a balanced gut microbiota [42–44]. SCFAs, especially butyrate, are known to enhance gut barrier integrity, reduce systemic inflammation, and regulate lipid and glucose metabolism [45–47]. Thus, the observed shift in gut microbiota composition suggests that FTM may improve metabolic health by promoting the growth of SCFA-producing bacteria, which in turn positively influence metabolic pathways and reduce inflammation.

While *Akkermansia* is typically regarded as a beneficial bacterium in the context of gut health and it can regulate metabolic functions such as improving insulin sensitivity and reducing obesity-related inflammation [48–50], emerging evidence suggests that its overgrowth in conditions of dysbiosis can contribute to increased gut permeability and systemic inflammation, thereby exacerbating metabolic disorders [51]. In this study, FTM treatment resulted in a significant reduction in *Akkermansia*

abundance, which may be an important mechanism underlying the observed improvements in metabolic health. These findings suggest that FTM's ability to reduce *Akkermansia* abundance may help restore gut homeostasis and mitigate the negative metabolic effects associated with its overgrowth. This observation further emphasizes the importance of maintaining a balanced gut microbiota. While *Akkermansia* may confer health benefits in normal conditions, its excessive proliferation under conditions of metabolic stress appears to exacerbate metabolic dysfunction. By regulating *Akkermansia* levels and promoting the growth of beneficial taxa, FTM appears to play a critical role in maintaining gut microbial balance, which is essential for overall metabolic health.

The phytochemical characterization of the FTM aqueous extract identified eight structurally distinct cevanine-type steroidal alkaloids, including both aglycones (e.g., peimine, peiminine, peimisine, isoverticine, ebeiedinone) and glycosylated forms (e.g., peimisine-3-β-D-glucoside, puqietinonoside, puqiedine). This diverse alkaloid profile underscores the extract's polypharmacological potential and provides a mechanistic foundation for the systemic effects observed in vivo.

Among these constituents, peimine and peiminine are the most extensively studied and are known to exhibit anti-inflammatory and antioxidative activities. These compounds have been reported to inhibit NF-κB and MAPK signaling, reduce proinflammatory cytokine release, and alleviate tissue damage in models of metabolic and inflammatory diseases [6, 52, 53]. Their actions are consistent with the transcriptional suppression of inflammatory genes and histological improvements in liver and pancreas tissues observed in this study. Furthermore, recent evidence suggests that peiminine can activate the SIRT1–AMPK axis, thereby promoting lipid oxidation and improving insulin sensitivity in hepatocytes [54, 55], providing a plausible link to the gene expression profiles associated with glucose and lipid metabolism.

Glycosylated alkaloids such as peimisine-3-β-D-glucoside and puqietinonoside may offer enhanced solubility and gastrointestinal stability and are subject to microbial hydrolysis in the gut. These biotransformations can release bioactive aglycones capable of modulating nuclear receptors involved in metabolic regulation, such as FXR, PPARα, or LXR, thereby influencing bile acid metabolism, lipid transport, and glucose homeostasis [56]. Isoverticine and ebeiedinone, though less characterized, are structurally similar to known smooth muscle relaxants and antioxidants and may contribute to microvascular protection and redox modulation under metabolic stress [57].

Importantly, the presence of multiple active compounds in FTM suggests a synergistic interaction across metabolic, inflammatory, and redox pathways. Rather than acting through a single target, the observed benefits likely arise from the convergence of these alkaloids on complementary molecular nodes. This multicomponent, multitarget mode of action is characteristic of medicinal plants with dual nutritional and therapeutic properties and supports the use of FTM as a functional food for managing complex metabolic disturbances.

Despite the promising results of this study, several limitations warrant consideration. While our study provides strong evidence for the modulation of gut microbiota by FTM, the precise molecular mechanisms underlying these changes remain unclear. Future research should focus on elucidating the specific pathways through which FTM influences microbial composition, particularly the role of SCFAs, and how these changes affect host metabolic pathways involved in lipid and glucose metabolism. Furthermore, although the results from our murine model are encouraging, the translation of these findings to human clinical settings remains to be confirmed. Long-term clinical trials are necessary to assess the safety, efficacy, and optimal dosing of FTM in humans [58], particularly in individuals with metabolic disorders such as obesity, type 2 diabetes, and nonalcoholic fatty liver disease. These studies will be pivotal in validating the therapeutic potential of FTM and determining its role in clinical practice.

The findings of this study are based on a HSFD-induced obesity model in male KM mice. While the results are relevant to understanding metabolic disturbances associated with diet-induced obesity, their generalization to other species or experimental conditions should be approached with caution. Differences in metabolic responses between species, such as humans, may exist due to variations in physiology and gut microbiota composition. However, the mechanisms explored, particularly the modulation of metabolic and inflammatory pathways by FTM, may offer insights into potential therapeutic strategies for human metabolic disorders, especially those related to obesity and insulin resistance.

In this study, we used only male KM mice, which may introduce a sex bias. Although male mice are commonly used in metabolic disease models to reduce experimental variability due to hormonal fluctuations, this single-sex design may not fully reflect sex differences in metabolic responses. Existing research indicates that sex significantly affects metabolic processes, and female mice, due to their hormonal cycles, may exhibit different physiological and metabolic responses compared to males [59]. Therefore, future studies should consider including female mice to assess sex-specific effects on metabolic diseases, thus providing more comprehensive and generalizable results. We acknowledge this limitation in our experimental design and suggest that subsequent research includes sex as a variable to more accurately reveal sex differences in metabolic responses.

Finally, while gut microbiota modulation represents a central mechanism in FTM's effects, future studies should also investigate other potential molecular pathways, including the regulation of inflammatory signaling, oxidative stress, and gut-derived metabolites. A deeper understanding of these pathways will provide a more comprehensive view of how FTM exerts its therapeutic effects and will help optimize its use for the treatment of metabolic diseases.

5. Conclusion

This study provides comprehensive evidence that FTM aqueous extract mitigates HSFD-induced metabolic

dysfunction through the integrated regulation of hepatic metabolism, inflammatory signaling, and gut microbiota composition. The extract reprogrammed key metabolic genes involved in lipid synthesis, insulin signaling, and immune modulation, while UPLC-QTOF-MS identified eight cevanine-type alkaloids that may act as core bioactive constituents. Furthermore, FTM treatment restored gut microbial diversity and enriched taxa associated with SCFA production and metabolic homeostasis. The convergence of transcriptional, microbial, and phytochemical findings reveals that FTM acts on the liver–gut–microbiota axis through a multitarget, multicomponent pharmacological mechanism. These results not only support the potential of FTM as a functional food but also provide a scientific foundation for its clinical translation in the prevention and adjunctive management of metabolic syndromes.

Data Availability Statement

The data that support the findings of this study are available from the corresponding author upon reasonable request.

Ethics Statement

All animal experiments were conducted in accordance with the ARRIVE guidelines. All animal testing procedures were approved by the Laboratory Animal Ethics Committee of Tianjin University of Traditional Chinese Medicine (No. TCM-LAEC2023211z1516, Tianjin, China). The full ARRIVE checklist is included in the Supporting Information to ensure full transparency in reporting of animal experiments.

Conflicts of Interest

The authors declare no conflicts of interest.

Author Contributions

Linen Zou: writing–original draft, software, investigation, data curation, and methodology. Yu Fu: investigation, data curation, and methodology. Lanna Wu: investigation and data curation. Jiale Cheng: visualization and data curation. Yanan Yang: writing—review and editing. Mingxi Li: writing–review and editing. Yuru Xu: methodology. Yan Jiang: investigation. Qingchun Wang: writing–review and editing, funding acquisition, and conceptualization. Chongming Wu: writing–review and editing, writing–original draft, supervision, and conceptualization. Linen Zou and Yu Fu contributed equally to this work.

Funding

This work was supported by grants from the following projects: (1) The Central Government Guiding Special Funds for Development of Local Science and Technology (NO. 2021ZY0046), (2) "First-class Discipline" Research Capacity Enhancement Project in Mongolian Pharmacy of Inner Mongolia Medical University (NO. MYX2023-K02), and (3) Science and Technology Program of Inner Mongolia (NO. 2021GG0126).

Acknowledgments

We used ChatGPT-4.0 solely for language editing and carefully reviewed the content to ensure its accuracy.

Supporting Information

Additional supporting information can be found online in the Supporting Information section. *(Supporting Information)*

This section includes supporting information such as the chemical structures of compounds (Figure S1); extracted ion chromatograms (Figure S2); and primer sequences for RT-qPCR analysis (Table S1); additionally, the ARRIVE Guidelines Author Checklist is provided to ensure comprehensive reporting of animal research, covering study design, sample size, randomization, blinding, and statistical methods.

References

[1] Y. H. Liu, K. Bei, W. R. Zheng, G. G. Yu, and C. X. Sun, "Assessment of Health Risks Associated With Pesticide and Heavy Metal Contents in Fritillaria Thunbergii Miq," *Environmental Science and Pollution Research* 30, no. 10 (2023): 26807–26818, https://doi.org/10.1007/s11356-022-23995-6.

[2] S. J. Wang, W. Y. Gao, H. X. Chen, and P. G. Xiao, "New Starches From Fritillaria Species Medicinal Plants," *Carbohydrate Polymers* 61, no. 1 (2005): 111–114, https://doi.org/10.1016/j.carbpol.2005.03.017.

[3] I. Rashid and U. Yaqoob, "Traditional Uses, Phytochemistry and Pharmacology of Genus Fritillaria—A Review," *Bulletin of the National Research Centre* 45 (2021): 1–124, https://doi.org/10.1186/s42269-021-00577-z.

[4] J. Xu, W. Zhao, L. Pan, et al., "A Main Active Ingredient of Fritillaria, Exhibits Anti-Inflammatory and Pain Suppression Properties at the Cellular Level," *Fitoterapia* 111 (2016): 1–6, https://doi.org/10.1016/j.fitote.2016.03.018.

[5] Z. Luo, B. Zheng, B. Jiang, X. Xue, E. Xue, and Y. Zhou, "Peiminine Inhibits the IL-1β Induced Inflammatory Response in Mouse Articular Chondrocytes and Ameliorates Murine Osteoarthritis," *Food & Function* 10, no. 4 (2019): 2198–2208, https://doi.org/10.1039/c9fo00307j.

[6] C. Liu, D. Zhen, H. Du, et al., "Synergistic Anti-Inflammatory Effects of Peimine, Peiminine, and Forsythoside a Combination on LPS-Induced Acute Lung Injury by Inhibition of the IL-17-NF-κB/MAPK Pathway Activation," *Journal of Ethnopharmacology* 295 (2022): 115343, https://doi.org/10.1016/j.jep.2022.115343.

[7] J. Chen, "Essential Role of Medicine and Food Homology in Health and Wellness," *Chinese Herbal Medicine* 15, no. 3 (2023): 347–348, https://doi.org/10.1016/j.chmed.2023.05.001.

[8] X. Fan, Y. Wang, X. Li, T. Zhong, C. Cheng, and Y. Zhang, "Scutellarin Alleviates Liver Injury in Type 2 Diabetic Mellitus by Suppressing Hepatocyte Apoptosis in Vitro and in Vivo," *Chinese Herbal Medicine* 15, no. 4 (2023): 542–548, https://doi.org/10.1016/j.chmed.2023.03.007.

[9] P. J. Turnbaugh, R. E. Ley, M. A. Mahowald, V. Magrini, E. R. Mardis, and J. I. Gordon, "An Obesity-Associated Gut Microbiome With Increased Capacity for Energy Harvest," *Nature* 444, no. 7122 (2006): 1027–1031, https://doi.org/10.1038/nature05414.

[10] P. D. Cani, J. Amar, M. A. Iglesias, et al., "Metabolic Endotoxemia Initiates Obesity and Insulin Resistance," *Diabetes* 56, no. 7 (2007): 1761–1772, https://doi.org/10.2337/db06-1491.

[11] H. Li, Y. Du, H. Ji, et al., "Adenosine-Rich Extract of Ganoderma Lucidum: A Safe and Effective Lipid-lowering Substance," *iScience* 25 (2022): 11–105214, https://doi.org/10.1016/j.isci.2022.105214.

[12] Y. N. Yang, Q. C. Wang, W. Xu, J. Yu, H. Zhang, and C. Wu, "The Berberine-Enriched Gut Commensal *Blautia producta* Ameliorates High-Fat Diet (HFD)-Induced Hyperlipidemia and Stimulates Liver LDLR Expression," *Biomedicine & Pharmacotherapy* 155 (2022): 113749, https://doi.org/10.1016/j.biopha.2022.113749.

[13] M. Vacca, G. Celano, F. M. Calabrese, P. Portincasa, M. Gobbetti, and M. De Angelis, "The Controversial Role of Human Gut Lachnospiraceae," *Microorganisms* 8 (2020): 4, https://doi.org/10.3390/microorganisms8040573.

[14] A. Koh, F. De Vadder, P. Kovatcheva-Datchary, and F. Bäckhed, "From Dietary Fiber to Host Physiology: Short-Chain Fatty Acids as Key Bacterial Metabolites," *Cell* 165, no. 6 (2016): 1332–1345, https://doi.org/10.1016/j.cell.2016.05.041.

[15] S. Zhong, Y. Q. Sun, J. X. Huo, et al., "The Gut Microbiota-Aromatic Hydrocarbon Receptor (AhR) Axis Mediates the Anticolitic Effect of Polyphenol-Rich Extracts From Sanghuangporus," *iMeta* 3, no. 2 (2024): 2-e180, https://doi.org/10.1002/imt2.180.

[16] L. E. Zou, Y. N. Yang, J. Zhan, et al., "Gut Microbiota-Based Discovery of Houttuyniae Herba as a Novel Prebiotic of Bacteroides Thetaiotaomicron With Anti-Colitis Activity," *Biomedicine & Pharmacotherapy* 172 (2024): 116302, https://doi.org/10.1016/j.biopha.2024.116302.

[17] W. Xu, J. Yu, Y. Yang, et al., "Strain-Level Screening of Human Gut Microbes Identifies Blautia Producta as a New Anti-Hyperlipidemic Probiotic," *Gut Microbiota* 15 (2023): 1–2228045, https://doi.org/10.1080/19490976.2023.2228045.

[18] W. H. Chang, J. Guo, Y. A. Yang, et al., "Semen Trigonellae Alleviates LPS-Induced Depressive Behavior via Enhancing the Abundance of Ligilactobacillus spp," *Food Science & Nutrition* 12, no. 11 (2024): 9414–9427, https://doi.org/10.1002/fsn3.4475.

[19] E. E. Canfora, R. C. R. Meex, K. Venema, and E. E. Blaak, "Gut Microbial Metabolites in Obesity, NAFLD and T2DM," *Nature Reviews Endocrinology* 15, no. 5 (2019): 261–273, https://doi.org/10.1038/s41574-019-0156-z.

[20] E. S. Chambers, T. Preston, G. Frost, and D. J. Morrison, "Role of Gut Microbiota-Generated Short-Chain Fatty Acids in Metabolic and Cardiovascular Health," *Current Nutrition Reports* 7, no. 4 (2018): 198–206, https://doi.org/10.1007/s13668-018-0248-8.

[21] J. Li, S. Yang, R. Lei, et al., "Oral Administration of Rutile and Anatase TiO(2) Nanoparticles Shifts Mouse Gut Microbiota Structure," *Nanoscale* 10, no. 16 (2018): 7736–7745, https://doi.org/10.1039/c8nr00386f.

[22] C. Zhang, G. Wang, X. Yin, et al., "Hepatic Protein Phosphatase 1 Regulatory Subunit 3G Alleviates Obesity and Liver Steatosis by Regulating the Gut Microbiota and Bile Acid Metabolism," *Journal of Pharmaceutical and Biomedical Analysis* 14 (2024): 8–100976, https://doi.org/10.1016/j.jpha.2024.100976.

[23] N. Wang, Y. Dilixiati, L. Xiao, H. Yang, and Z. Zhang, "Different Short-Chain Fatty Acids Unequally Modulate Intestinal Homeostasis and Reverse Obesity-Related Symptoms in Lead-Exposed High-Fat Diet Mice," *Journal of Agricultural and Food Chemistry* 72, no. 34 (2024): 18971–18985, https://doi.org/10.1021/acs.jafc.4c04193.

[24] W. Zhang, M. Zhu, X. Liu, et al., "Edible Bird's Nest Regulates Glucose and Lipid Metabolic Disorders via the gut-liver Axis in Obese Mice," *Food & Function* 15, no. 14 (2024): 7577–7591, https://doi.org/10.1039/d4fo00563e.

[25] M. Y. Yang, Y. J. Liu, M. H. Zheng, et al., "Anti-Adipogenesis and Anti-Obesity Potential of Alliin Mediated by Modulating Glycolipid Metabolism via Activating PPARγ Signaling," *Naunyn-Schmiedeberg's Archives of Pharmacology* 397, no. 11 (2024): 8707–8723, https://doi.org/10.1007/s00210-024-03181-w.

[26] K. J. Jeong, G. W. Kim, and S. H. Chung, "AMP-Activated Protein Kinase: An Emerging Target for Ginseng," *Journal of Ginseng Research* 38, no. 2 (2014): 83–88, https://doi.org/10.1016/j.jgr.2013.11.014.

[27] H. N. Mu, Q. Zhou, R. Y. Yang, et al., "Caffeic Acid Prevents Non-Alcoholic Fatty Liver Disease Induced by a High-Fat Diet Through Gut Microbiota Modulation in Mice," *Food Research International* 143 (2021): 110240, https://doi.org/10.1016/j.foodres.2021.110240.

[28] D. C. Cominguez, Y. J. Park, Y. M. Kang, A. Nugroho, S. Kim, and H. J. An, "Clitorin Ameliorates Western Diet-Induced Hepatic Steatosis by Regulating Lipogenesis and Fatty Acid Oxidation in Vivo and in Vitro," *Scientific Reports* 12 (2022): 1–4154, https://doi.org/10.1038/s41598-022-07937-3.

[29] H. Zeng, H. Qin, M. Liao, et al., "CD36 Promotes De Novo Lipogenesis in Hepatocytes Through INSIG2-Dependent SREBP1 Processing," *Molecular Metabolism* 57 (2022): 101428, https://doi.org/10.1016/j.molmet.2021.101428.

[30] Y. Shi, R. Guo, X. Wang, et al., "The Regulation of Alfalfa Saponin Extract on Key Genes Involved in Hepatic Cholesterol Metabolism in Hyperlipidemic Rats," *PLoS One* 9 (2014): 2–e88282, https://doi.org/10.1371/journal.pone.0088282.

[31] H. Ou, Q. Zhang, and J. Zeng, "Improving Lipoprotein Profiles by Liver-Directed Gene Transfer of Low Density Lipoprotein Receptor Gene in Hypercholesterolaemia Mice," *Journal of Genetics* 95, no. 2 (2016): 311–316, https://doi.org/10.1007/s12041-016-0636-z.

[32] Z. H. Yang, K. Nill, Y. Takechi-Haraya, et al., "Differential Effect of Dietary Supplementation With a Soybean Oil Enriched in Oleic Acid Versus Linoleic Acid on Plasma Lipids and Atherosclerosis in LDLR-Deficient Mice," *International Journal of Molecular Sciences* 23 (2022): 15, https://doi.org/10.3390/ijms23158385.

[33] C. Kang and L. Li Ji, "Role of PGC-1α Signaling in Skeletal Muscle Health and Disease," *Annals of the New York Academy of Sciences* 1271, no. 1 (2012): 110–117, https://doi.org/10.1111/j.1749-6632.2012.06738.x.

[34] S. Rius-Pérez, I. Torres-Cuevas, I. Millán, L. Ortega Á, and S. Pérez, "PGC-1α, Inflammation, and Oxidative Stress: An Integrative View in Metabolism," *Oxidative Medicine and Cellular Longevity* 2020 (2020): 1452696, https://doi.org/10.1155/2020/1452696.

[35] Y. M. Wan, H. M. Wu, Y. H. Li, et al., "TSG-6 Inhibits Oxidative Stress and Induces M2 Polarization of Hepatic Macrophages in Mice With Alcoholic Hepatitis via Suppression of STAT3 Activation," *Frontiers in Pharmacology* 11 (2020): 10, https://doi.org/10.3389/fphar.2020.00010.

[36] X. Zhang, T. Weiß, M. H. Cheng, et al., "Structural Basis of CMKLR1 Signaling Induced by chemerin9" (2023), https://doi.org/10.1101/2023.06.09.544295.

[37] Z. Hu, G. Chen, C. Yan, et al., "Autophagy Affects Hepatic Fibrosis Progression by Regulating Macrophage Polarization and Exosome Secretion," *Environmental Toxicology* 38, no. 7 (2023): 1665–1677, https://doi.org/10.1002/tox.23795.

[38] H. Shi, M. V. Kokoeva, K. Inouye, I. Tzameli, H. Yin, and J. S. Flier, "TLR4 Links Innate Immunity and Fatty Acid-Induced Insulin Resistance," *Journal of Clinical Investigation* 116, no. 11 (2006): 3015–3025, https://doi.org/10.1172/jci28898.

[39] N. Cai, W. Zhou, L. L. Ye, et al., "The STAT3 Inhibitor Pimozide Impedes Cell Proliferation and Induces ROS Generation in Human Osteosarcoma by Suppressing Catalase Expression," *American Journal of Translational Research* 9 (2017): 3853–3866.

[40] O. Abu Shelbayeh, T. Arroum, S. Morris, and K. B. Busch, "PGC-1α is a Master Regulator of Mitochondrial Lifecycle and ROS Stress Response," *Antioxidants* 12 (2023): 5, https://doi.org/10.3390/antiox12051075.

[41] D. Alkazemi, A. Rahman, and B. Habra, "Alterations in Glutathione Redox Homeostasis Among Adolescents With Obesity and Anemia," *Scientific Reports* 11 (2021): 1–3034, https://doi.org/10.1038/s41598-021-82579-5.

[42] D. Parada Venegas, M. K. De la Fuente, G. Landskron, et al., "Short Chain Fatty Acids (SCFAs)-Mediated Gut Epithelial and Immune Regulation and Its Relevance for Inflammatory Bowel Diseases," *Frontiers in Immunology* 10 (2019): 277, https://doi.org/10.3389/fimmu.2019.00277.

[43] L. Ma, Y. Ni, Z. Wang, et al., "Spermidine Improves Gut Barrier Integrity and Gut Microbiota Function in Diet-Induced Obese Mice," *Gut Microbes* 12 (2020): 1–19, https://doi.org/10.1080/19490976.2020.1832857.

[44] G. Mao, S. Li, C. Orfila, et al., "Depolymerized RG-I-enriched Pectin From Citrus Segment Membranes Modulates Gut Microbiota, Increases SCFA Production, and Promotes the Growth of Bifidobacterium spp., Lactobacillus spp. and Faecalibaculum spp," *Food & Function* 10, no. 12 (2019): 7828–7843, https://doi.org/10.1039/c9fo01534e.

[45] J. He, P. Zhang, L. Shen, et al., "Short-Chain Fatty Acids and Their Association With Signalling Pathways in Inflammation, Glucose and Lipid Metabolism. Secondary Short-Chain Fatty Acids and Their Association With Signalling Pathways in Inflammation," *Glucose and Lipid Metabolism* 21 (2020): 17, https://doi.org/10.3390/ijms21176356.

[46] C. Martin-Gallausiaux, L. Marinelli, H. M. Blottière, P. Larraufie, and N. Lapaque, "SCFA: Mechanisms and Functional Importance in the Gut," *Proceedings of the Nutrition Society* 80, no. 1 (2021): 37–49, https://doi.org/10.1017/s0029665120006916.

[47] E. E. Blaak, E. E. Canfora, S. Theis, et al., "Short Chain Fatty Acids in Human Gut and Metabolic Health," *Life* 11, no. 5 (2020): 411–455, https://doi.org/10.3920/bm2020.0057.

[48] C. Dong, J. Yu, Y. Yang, et al., "Berberine, A Potential Prebiotic to Indirectly Promote Akkermansia Growth Through Stimulating Gut Mucin Secretion," *Biomedicine & Pharmacotherapy* 139 (2021): 111595, https://doi.org/10.1016/j.biopha.2021.111595.

[49] Y. Yu, J. Lu, L. Sun, et al., "Akkermansia Muciniphila: A Potential Novel Mechanism of Nuciferine to Improve Hyperlipidemia," *Biomedicine & Pharmacotherapy* 133 (2021): 111014, https://doi.org/10.1016/j.biopha.2020.111014.

[50] A. Hasani, S. Ebrahimzadeh, F. Hemmati, A. Khabbaz, A. Hasani, and P. Gholizadeh, "The Role of Akkermansia muciniphila in Obesity, Diabetes and Atherosclerosis," *Journal of Medical Microbiology* 70 (2021): 10, https://doi.org/10.1099/jmm.0.001435.

[51] S. Qu, Y. Zheng, Y. Huang, et al., "Excessive Consumption of Mucin by Over-colonized Akkermansia muciniphila Promotes Intestinal Barrier Damage During Malignant Intestinal Environment," *Frontiers in Microbiology* 14 (2023): 1111911, https://doi.org/10.3389/fmicb.2023.1111911.

[52] K. Chen, Z. T. Lv, C. H. Zhou, et al., "Peimine Suppresses Interleukin-1β-Induced Inflammation via MAPK Down-regulation in Chondrocytes," *International Journal of Molecular Medicine* 43, no. 5 (2019): 2241–2251, https://doi.org/10.3892/ijmm.2019.4141.

[53] P. F. Yi, Y. C. Wu, H. B. Dong, et al., "Peimine Impairs Pro-Inflammatory Cytokine Secretion Through the Inhibition of the Activation of NF-κB and MAPK in LPS-Induced RAW264.7 Macrophages," *Immunopharmacology and Immunotoxicology* 35, no. 5 (2013): 567–572, https://doi.org/10.3109/08923973.2013.822508.

[54] X. Hou, S. Xu, K. A. Maitland-Toolan, et al., "SIRT1 Regulates Hepatocyte Lipid Metabolism Through Activating AMP-Activated Protein Kinase," *Journal of Biological Chemistry* 283, no. 29 (2008): 20015–20026, https://doi.org/10.1074/jbc.M802187200.

[55] F. Qi, T. Li, Q. Deng, and A. Fan, "The Impact of Aerobic and Anaerobic Exercise Interventions on the Management and Outcomes of Non-Alcoholic Fatty Liver Disease," *Physiological Research* 73, no. 5/2024 (2024): 671–686, https://doi.org/10.33549/physiolres.935244.

[56] S. Gao and M. Hu, "Bioavailability Challenges Associated With Development of Anti-Cancer Phenolics," *Mini-Reviews in Medicinal Chemistry* 10, no. 6 (2010): 550–567, https://doi.org/10.2174/138955710791384081.

[57] C. Liu, X. Zhu, E. Aga, et al., "Ebeiedinone and Peimisine Inhibit Cigarette Smoke extract-induced Oxidative Stress Injury and Apoptosis in BEAS-2B Cells," *Cell Stress and Chaperones* 29, no. 6 (2024): 697–708, https://doi.org/10.1016/j.cstres.2024.10.001.

[58] D. Zhu, W. Wang, G. Tong, et al., "Efficacy and Safety of GLP-1 Analog Ecnoglutide in Adults with Type 2 Diabetes: a Randomized, double-blind, placebo-controlled Phase 2 Trial," *Nature Communications* 15 (2024): 1–8408, https://doi.org/10.1038/s41467-024-52353-y.

[59] F. Mauvais-Jarvis, A. P. Arnold, and K. Reue, "A Guide for the Design of Pre-Clinical Studies on Sex Differences in Metabolism," *Cell Metabolism* 25, no. 6 (2017): 1216–1230, https://doi.org/10.1016/j.cmet.2017.04.033.